Evidence of Histone H2A.Z Deacetylation and Cardiomyocyte Dedifferentiation in Infarcted/Tip60-depleted Hearts

Xinrui Wang[1,3], Katherine Kulik[2,3], Tina C. Wan[1,3],
John W. Lough[2,3*], John A. Auchampach[1,3*]

[1]Department of Pharmacology and Toxicology
[2]Department of Cell Biology Neurobiology and Anatomy
[3]Cardiovascular Center
Medical College of Wisconsin
Milwaukee, WI 53226

*Co-corresponding authors

Number of Figures: 9

Number of Tables: 0

Number of Supplemental Figures: 7

Number of Supplemental Tables: 1

Key Words: Cardiomyocyte, Dedifferentiation, Histone H2A.Z, Myocardial Infarction, Tip60

Financial Support: NHLBI 5R01HL131788 (JAA & JWL) and American Heart Association Postdoctoral Fellowship #828662 (XW).

Running Title: H2A.Z deacetylation/dedifferentiation in Tip60-depleted cardiomyocytes

Co-Corresponding Authors: John A. Auchampach, PhD
Department of Pharmacology & Toxicology
Medical College of Wisconsin
8701 Watertown Plank Road
Milwaukee, Wisconsin 53226
Phone: 414-955-5643
Email: jauchamp@mcw.edu

John W. Lough, PhD
Department of Cell Biology, Neurobiology & Anatomy
Medical College of Wisconsin
8701 Watertown Plank Road
Milwaukee, Wisconsin 53226
Phone: 414-955-8459
Email: jlough@mcw.edu

Non-Standard Abbreviations: CM, cardiomyocyte; cTnT, cardiac troponin-T; H2A.Zac$^{K4/K7}$, histone H2A.Z acetylated at lysines 4 and 7; Kat5, lysine acetyltransferase-5 (Tip60); MI, myocardial infarction; Nkx2.5, homeobox protein Nkx2-5; Tip60, Tat-interactive protein 60 kD; WGA, wheat germ agglutinin

Author Contributions: XW, JWL, and JAA designed the study. XW, KK, and TCW performed the experiments. XW, JWL, and JAA analyzed data, prepared figures, and wrote the manuscript. All authors reviewed, revised, and approved the final version.

Conflicts of Interest: none declared.

ABSTRACT

Myocardial infarction (MI) in the human heart causes death of billions of cardiomyocytes (CMs), resulting in cardiac dysfunction that is incompatible with life or lifestyle. In order to re-muscularize injured myocardium, replacement CMs must be generated via renewed proliferation of surviving CMs. Approaches designed to induce proliferation of CMs after injury have been insufficient. Toward this end, we are targeting the Tip60 acetyltransferase, based on the rationale that its pleiotropic functions conspire to block the CM cell-cycle at several checkpoints. We previously reported that genetic depletion of Tip60 in a mouse model after MI reduces scarring, retains cardiac function, and activates the CM cell-cycle, although it is unclear whether this culminates in the generation of daughter CMs. For pre-existing CMs in the adult heart to resume proliferation, it is becoming widely accepted that they must first dedifferentiate, a process highlighted by loss of maturity, epithelial to mesenchymal transitioning (EMT), and reversion from fatty acid oxidation to glycolytic metabolism, accompanied by softening of the myocardial extracellular matrix. Findings in hematopoietic stem cells, and more recently in neural progenitor cells, have shown that Tip60 induces and maintains the differentiated state via site-specific acetylation of the histone variant H2A.Z. Here, we report that genetic depletion of Tip60 from naïve or infarcted hearts results in the near-complete absence of acetylated H2A.Z in CM nuclei, and that this is accordingly accompanied by altered gene expressions indicative of EMT induction, ECM softening, decreased fatty acid oxidation, and depressed expression of genes that regulate the TCA cycle. These findings, combined with our previous work, support the notion that because Tip60 has multiple targets that combinatorially maintain the differentiated state and inhibit proliferation, its transient therapeutic targeting to ameliorate the effects of cardiac injury should be considered.

INTRODUCTION

The burden of ischemic heart disease remains large, with myocardial infarction (MI) and heart failure (HF) accounting for nearly 15% of deaths in the U. S. [1]. Because billions of cardiomyocytes (CMs) are lost during MI, the goal of protecting and re-muscularizing the myocardium constitutes an urgent clinical challenge. The mitigation of cardiac dysfunction caused by cardiomyocyte (CM) loss and replacement with scar tissue after MI requires the regeneration of lost CMs, i.e. re-muscularization. Unlike most organs, the adult heart cannot generate replacement CMs because these cells have evolved to reside in a profound state of proliferative senescence, which becomes established soon after birth.

With the goal of releasing surviving CMs from their non-proliferative state, research during the past decade has targeted proteins that either induce or inhibit CM proliferation, via over-expression or knock-out of pro-growth genes in mouse models (review, [2]). Although these studies have shown that the cell-cycle in CMs can be reactivated when targeting individual genes, the extent of remuscularization and functional improvement in most cases is minimal, which is not surprising considering the variety of inhibitors that have evolved to prevent CMs from dividing. In order to disengage this inhibitory network following MI, we are targeting the acetyltransferaseTip60, per a rationale based on findings from *in vitro* studies showing that Tip60 is pleiotropic, acetylating proteins that block the cell-cycle at three checkpoints: (i) G_1/S, by maintaining p21 at inhibitory levels, [3, 4]; (ii) G_2/M, by activating Atm to induce the DNA damage response (DDR; [5]), and (iii) cytokinesis, via acetylation of Aurkb [6]; also, because it is well-established that Tip60-mediated acetylation of p53 is pro-apoptotic [7-9], its targeting is cardioprotective. Consistent with these prior studies, our recent findings using an *in vivo* Tip60 knockout model have shown that genetic depletion of Tip60 from CMs after MI in the mouse heart restores left ventricular (LV) systolic function to near pre-MI baseline values, concomitant with reduced apoptosis and scarring, as well as cell-cycle activation [10, 11]. These results are phenocopied by administering drugs that inhibit Tip60's acetyltransferase activity [12]. However, it remains unknown whether activation of the CM cell-cycle subsequent to depletion of Tip60 results in bona fide proliferation, i.e. the generation of new daughter CMs, thereby fulfilling a major challenge in the field of cardiac regeneration.

In this regard, recent findings in other laboratories have strongly supported the notion that in order to proliferate, mature adult CMs must 'dedifferentiate' [13, 14], a process in which the expression of 'adult' genes is diminished as 'embryonic' genes are re-expressed. CM dedifferentiation is highlighted by cell-cycle activation [13-15], an epithelial-to-mesenchymal transition (EMT; [16]), softening of the myocardial extracellular matrix (ECM) [15, 17-20], and as recently reported the inhibition of fatty acid oxidation [21]. The dedifferentiation process in CMs is the subject of a recent review [22]. Here, we report that depletion of Tip60 after MI is accompanied by the near-complete loss of the histone variant H2A.Z that is acetylated at lysines K4 and K7, hereafter denoted H2A.Zac$^{K4/K7}$, in CMs, a Tip60-mediated epigenetic modification recently shown to be required to maintain the differentiated state of hematopoietic stem cells (HSCs, [23]), as well as of skeletal myocytes and neurons [24]. Accordingly, we also show that depletion of Tip60 in CMs after MI alters the expression of genes indicative of the dedifferentiation process. Interpreted in accord with our previous findings [10, 11], these results suggest that depletion of Tip60 after MI may permit the resumption of CM proliferation by initiating dedifferentiation, as well as by de-inhibiting cell-cycle blockers including p21 and Atm. These findings further support the idea that clinical targeting of Tip60 to prevent acetylation of its multiple targets that prevent proliferation can promote myocardial regeneration post-MI.

MATERIALS AND METHODS

Animal Care & Experimentation: These experiments adhered to the National Institutes of Health (NIH) Guide for the Care and Use of Laboratory Animals (NIH Pub. Nos. 85-23, Revised 1996). All protocols are described in an Animal Use Application (AUA #000225) approved by the Medical College of Wisconsin Institutional Animal Care and Use Committee (IACUC), which possesses Animal Welfare Assurance status from the Office of Laboratory Animal Welfare (A3102-01).

Preparation of the mouse model used in these experiments wherein exons 3-11 of the *Kat5* gene encoding Tip60 are floxed, comprising two-thirds of the coding sequence including the chromo and acetyltransferase domains, was previously described [25]. These mice were mated with mice containing an α-myosin heavy chain (*Myh6*)-driven *MerCreMer-recombinase* transgene (Jackson Laboratory #005650), the Cre recombinase product of which, upon administration of tamoxifen, translocates from the cytoplasm to the nucleus to recombine floxed alleles [26]. All mice were on a mixed B6/sv129 genetic background. Experimental groups contained equal numbers of adult (10-14 weeks-old) males and females.

To ablate floxed *Kat5* alleles, mice received a daily intraperitoneal injection of tamoxifen (40 mg/kg [Sigma #T5648] suspended with 5% ethanol in sunflower oil) for three consecutive days. In experiments involving myocardial infarction (MI; described in detail below), tamoxifen was intra-peritoneally administered on three consecutive days, beginning on the third day after inducing MI via ligation of the left main coronary artery. On the day before harvest (i.e., 14 days post-MI), mice were injected intraperitoneally with BrdU (1 mg). On the day of harvest, mice were euthanized with CO_2, followed by removal of hearts and processing components for isolating total RNA, for which tissue between the base and ~1 mm above the suture was utilized, and immunostaining/protein isolation, for which tissue ~1 mm above the suture to the apex was utilized. Tissue samples for RNA and protein isolation were respectively placed in TRIzol (Thermo-Fisher #15596026), and Histone Extraction Buffer (Active Motif #37513) containing Halt's protease/phosphatase inhibitor cocktail (Thermo-Fisher #78440) with deacetylase inhibitors (MedChemExpress #HY-K0030), minced, homogenized with a teflon pestle, and stored at -80° C until further processing.

Myocardial Infarction: To induce MI, mice were anesthetized with isoflurane (1.0-1.5%) delivered via a nose cone, intubated and mechanically respirated (model 845, Harvard Apparatus) via an endotracheal tube with room air supplemented with 100% oxygen; to maintain anesthesia, isoflurane was delivered via the ventilator. The electrocardiogram (ECG; limb lead II configuration) was continuously recorded (Powerlab) using needle electrodes; rectal temperature was maintained at 37°C throughout the experiments using a servo-controlled heating pad. Before initiating surgery, mice were subcutaneously injected with sustained release meloxicam (4 mg/kg) to limit post-operative pain. Once anesthetized, thoracotomy was performed to the left of the sternum to expose the heart. This was followed by opening the pericardium, and, with assistance of a microscope, insertion of an 8.0 nylon suture beneath the left main coronary artery at a level below the tip of the left atrium; this placement was designed to target the lower half of the ventricle. Ischemia was then induced by ligating the suture with a double knot, after which coronary occlusion was verified by observation of myocardial blanching distal to the ligature, as well as by ST segment elevation per ECG. Following ligation, the chest wall was closed with polypropylene suture, and recovery was monitored until mice became fully ambulatory.

Genotyping: Genotyping was performed by PCR in 20 µl volume reactions that included 1x GoTaq Green Master Mix (Promega #M7123), 1.1 mM $MgCl_2$, 0.5 µM each primer, 0.5 µM internal control primers, and 4.0 µl template. Templates were from supernatants of ear tissue that had been boiled for 10 minutes in 0.3 mL 10 mM NaOH/1 mM EDTA. Sequences of primer pairs employed for PCR are listed in Supplemental Table 1. PCR products were amplified in an AB Applied Biosystems GeneAmp PCR System 9700 using the following programs: for LoxP, one 5-minute cycle at 95° C, thirty-five cycles at 94° C 30 sec/61° C 45 sec/72° C 45 sec, followed by one 10-minute cycle at 72° C; for *Myh6-MerCreMer*, one 5-minute cycle at 95° C, thirty-five cycles at 94° C 30 sec/54° C 45 sec/72° C 45 sec, followed by one 10-minute cycle at 72° C. Amplicons were separated at 100-110 V for one hour in 1% agarose/ethidium bromide and imaged.

RT-qPCR: Heart tissue, previously disrupted by homogenization with a motorized (Kimble 749540-0000) Teflon pestle and stored at -80° C in TRIzol reagent, was thawed. RNA was immediately purified using PureLink RNA

Mini-Kits (ThermoFisher #12183018A), including a genomic DNA removal step (PureLink DNase kit for on-column protocol, Thermo-Fisher #12185-010), according to the manufacturer's instructions. RNA yield & quality were determined via 260/280 ratio using Eppendorf Biophotometer Plus Instrument.

cDNA was synthesized as follows. After diluting an RNA sample from each heart so that precisely 1.0 µg was suspended in 14 µl nuclease-free distilled water (NFDW), 4.0 µl 5x VILO reaction mixture (ThermoFisher #11754050) were added. To start the reverse-transcription reaction, 2.0 µl 10x SuperScript Enzyme Mix (ThermoFisher #11754050) were added, followed by transfer to an Applied Biosystems Veriti 96-well Thermocycler programmed as follows: 10 minutes at 25° C, 60 minutes at 42° C, and 5 minutes at 85° C. cDNA templates were diluted with NFDW to a concentration of 3.125 ng/µl and stored at -20° C.

qPCR was carried-out by subjecting each biological replicate (i.e., sample from each individual heart) to triplicate determinations. Each reaction was performed in a total volume of 10 µl in 384-well arrays, each well containing 1x Taqman Fast-Advanced Master Mix (ThermoFisher #4444557), 1x Taqman Probe Kit (Supp. Table 1), and 12.5 ng cDNA as template. The arrayed samples were amplified in a Bio-Rad CFX384 Real Time System (C1000 Touch) programmed as follows: 2 minutes at 50° C, 20 seconds at 95° C, 3 seconds at 95° C, and 30 seconds at 60° C; the last two steps were repeated 39 times. Results were processed using Bio-Rad CFX Manager 3.1 software.

Western Blotting: Histones were purified from adult heart tissue using Active Motif's Histone Purification Mini Kit (cat. no. 40026), according to the manufacturer's recommendations which were modified as described below. All procedures were performed at 0-4 °C. Using a minimal volume of low pH Extraction Buffer, which contains protease and deacetylase inhibitors, 50mg tissue was completely dispersed using a Dounce homogenizer and a microtip sonicator, followed by centrifugation (5 min, 21,000g). Following adjustment of the supernatant to pH8.0 using 5X Neutralization Buffer, 'crude' histones were de-salted using a Zeba Spin Desalting Column (Thermo-Fisher #89883), after which Sample Buffer (Cell Signaling #12957) was added. For electrophoresis, a sample from each heart was loaded into individual lanes of a pre-cast Bio-Rad 4-20% acrylamide gel. After application of current (100 V) until the tracking dye reached the bottom of the gel, separated proteins were transferred (60 min at 100 V) onto 0.2 µm nitrocellulose membrane (Thermo-Fisher #88013). Blots were blocked with 5% non-fat dry milk/20 mM Tris (pH 7.6)/150 mM NaCl/0.1%Tween-20 (5% NFDM/TBST) or 5% BSA in TBST. Primary and secondary antibodies and dilutions are Acetyl-Histone H2A.Z (Lys4/Lys7, 1:1000, Cell Signaling #75336), Histone H2A.Z (1:1000, Active Motif #39013), and HRP-linked goat anti-rabbit (1:2000, Cell Signaling #7074). Blots were reacted with primary antibody in 5% NFDM/TBST or 5% BSA/TBST overnight at 4°C. Secondary antibodies were diluted in 5% BSA/TBST and applied for 60 minutes at RT. Reacted blots were covered with Pierce™ ECL horseradish peroxidase substrate (ThermoFisher #32209) for 1 min at room temperature, followed by chemiluminescence imaging and densitometry using Bio-Rad ChemiDoc and ImageJ software, respectively.

Immunostaining & Cell Counting: On the day before harvest, mice were injected with 1 mg 5'-bromo-2'-deoxyuridine (BrdU; Sigma #B9285). Following removal, hearts were perfused with ice-cold cardioplegic solution and atria were removed. Ventricles were fixed overnight in fresh ice-cold 4% paraformaldehyde/PBS, processed through ethanol series, and embedded in paraffin. Sections (4 µm thick) mounted on microscope slides were de-waxed, subjected to antigen retrieval (100°C in 10 mM trisodium citrate pH6.0/0.05% Tween-20 for 20 minutes) followed by 30 minutes' cooling at RT, and blocked with 2% goat or 5% donkey serum/0.1% Triton-X-100 in PBS. Primary antibodies against acetyl-Histone H2A.Z (Lys4/Lys7, 1:100, Cell Signaling #75336), Histone H2A.Z (1:200, Active Motif #39013), Nkx2.5 (1:250, Abcam #ab106923), cardiac Troponin-T (cTnT, 1:2000, Abcam #ab8295), α-smooth muscle actin (1:100, Dako #M0851), and H3K4^{me3} (1:600, Active Motif #39160) were diluted in blocking buffer and applied overnight at 4°C; secondary antibodies goat anti-rabbit 568 (1:500, Invitrogen #A-11036), goat anti-mouse 488 (1:500, Invitrogen #A-11029), donkey anti-rabbit 555 (1:500, Invitrogen #A-31572), and donkey anti-goat 488 (1:500, Invitrogen #A-32814) were applied for one hour in the dark.

Microscopy was performed using a Nikon Eclipse 50i microscope equipped with a Nikon DSU3 digital camera. During counting, at least 300 CMs were evaluated in 6 random 400x photomicrographic fields, identity of which were confirmed by immunostaining the cytoplasmic marker cardiac troponin-T (cTnT) or the nuclear marker Nkx2.5. Percentages of CMs expressing acetylated or bulk histone H2A.Z were assessed by monitoring fluorescent signal in the Texas Red channel, after confirming the identity of each stained CM in the FITC channel. To identify nuclei as acetylated or bulk histone H2A.Z -positive, only those at least half-filled with fluorescence

were counted; acetylated or bulk histone H2A.Z positive nuclei were also confirmed to be DAPI-positive. In infarcted hearts, acetylated or bulk histone H2A.Z immunoreactivity were assessed in both the remote zone, specifically the area of myocardium ~2 mm distal to the infarct boundary, and in the border zone, specifically the area immediately adjacent to the infarct zone. WGA staining was performed using Thermo-Fisher #W11263 Alexa Fluor 350 conjugate.

RNAseq: RNA quality was determined using an Agilent BioAnalyzer 2100. RNA libraries were prepared by BGI Americas. A total of 32 samples were tested for strand-specific mRNA sequencing on a DNBSEQ platform. SOAPnuke v1.5.2 was used to remove reads whose N content is greater than 5%, the reads containing the adaptor, and reads with low base quality (< 15). Filtered clean reads (>45 M per sample) were stored in FASTQ format and aligned to the *Mus musculus* genome (GCF 000001635.26 GRCm38.p6) using HISAT2 v 2 0.4. Bowtie2 was used to align clean reads to the reference genes. A total of 17,714 genes were detected. The average alignment ratio of the sample comparison genome was 96.63%. Gene expression levels were calculated by RSEM (v1.2.28) and quantified by fragments per kilobase of transcript per million reads mapped (FPKM). DEGs for each experimental group, as compared to control, were detected using DESeq2. The phyper function in R software is used for enrichment analysis and calculation of P values; Q values were obtained by correction of P value.

Statistics: The DEG heatmap was generated by the Dr.Tom platform (BGI Americas) according to the DESeq2 analysis results. GO enrichment analysis of annotated DEGs was performed by Phyper based on Hypergeometric test. The significant levels of terms and pathways were corrected by Q value with a rigorous threshold (Q value ≤ 0.05). All other determinations were performed in blinded fashion and are reported as means ±SEM, and compared by an unpaired, two-tailed Student's t test. $P<0.05$ was considered statistically significant.

RESULTS

Genetic Depletion of Tip60 in CMs Abolishes Acetylation of Histone H2A.Z.

In this study we compared 12 week-old adult control mice denoted *Kat5*$^{f/f}$ (i.e., *Kat5*$^{flox/flox}$) with experimentals designated *Kat5*$^{\Delta/\Delta}$ (i.e., *Kat5*$^{flox/flox;Myh6\text{-}merCremer}$), in which the *Kat5* gene encoding Tip60 was disrupted by injecting tamoxifen for three consecutive days to activate *Myh6*-driven Cre-recombinase. In infarcted hearts treated with tamoxifen for three days beginning on the third day post-MI, as well as in non-injured (naïve) hearts, expression of the *Kat5* gene was reduced by approximately 25%; by contrast, *Kat5* expression was unaffected in controls to assess off-target effects of Cre-recombinase (Supp. Fig. 1a). Using this model we recently reported that depletion of Tip60 after MI preserves cardiac function, reduces scarring, and re-initiates the cell-cycle in CMs of both neonatal [10] and adult hearts [27]. Here, as shown in Figure 1a, depletion of Tip60 (*Kat5*$^{\Delta/\Delta}$) in CMs of infarcted adult hearts resulted in the absence of acetylated histone H2A.Z, i.e, H2A.Zac$^{K4/K7}$, in nearly all CM nuclei. This was the most pronounced biochemical effect of Tip60 depletion that we have observed, in this as well as in our previous studies [10-12]. To verify that depletion of H2A.Zac$^{K4/K7}$ was confined to CM nuclei, CM identity was confirmed by immunostaining the nuclear marker Nkx2-5 (Supp. Fig. 2). By contrast, using an antibody that detects bulk (i.e., both acetylated and non-acetylated) H2A.Z, no effects of Tip60 depletion were seen (Supp. Fig. 3). Surprisingly, the percentage of H2A.Zac$^{K4/K7}$-positive nuclei of interstitial cells (i.e., non-CMs) was increased in both the infarct border and remote zones (Supp. Fig. 4). Also, CM-specific depletion of H2A.Zac$^{K4/K7}$ was not caused by an off-target effect of Cre-recombinase (Supp. Fig. 5). To verify reduction of H2A.Zac$^{K4/K7}$ in heart tissue wherein Tip60 was depleted in CMs, western blotting was performed. As shown in Figure 1b, despite blotting total proteins extracted from whole heart tissue wherein the majority of cells are non-CMs, levels of H2A.Zac$^{K4/K7}$ were markedly reduced (by ~two-thirds) when Tip60 was depleted, even though levels of bulk H2A.Z were modestly increased according to the quantitation of blots shown in Supp. Fig. 6.

Dysregulation of Genes Previously Associated with CM Dedifferentiation & Cell-Cycle Activation in Infarcted/Tip60-depleted Hearts

Based on findings that Tip60-mediated acetylation of H2A.Z sustains differentiation in HSCs [23] and neurons [24], combined with reports that adult CMs undergo dedifferentiation in order to permit resumption of cell-cycling and regeneration after myocardial injury [14-16, 28, 29], it was of interest to assess whether reduction of H2A.Zac$^{K4/K7}$ in CMs correlated with the altered expression of markers commonly associated with the dedifferentiation process. Hence, we assessed the global effects of depleting Tip60 at 14 days post-MI via RNAseq, which revealed marked overall effects wherein depletion of Tip60 in CMs of naive and infarcted hearts generated 3,242 and 4,049 differentially expressed genes (DEGs), respectively, with minimal effects (i.e., 88 DEGs) of Cre-recombinase (Supp Fig. 1b-c).

As shown in Figure 2a, genes within the GO Term 'Cell Cycle' were both up- and down-regulated in infarcted/Tip60-depleted hearts at day 14 post-MI; regarding possible effects of Cre, a subset of genes mildly up-regulated by Cre was curiously inhibited when Tip60 was depleted (see Discussion). Remarkably, consistent with our recently reported findings that genetic depletion of Tip60 in CMs re-activates the cell-cycle [10, 27], RNAseq (Fig. 2b) and RT-qPCR (Fig. 2c) data indicated that this was associated with the up-regulation of genes encoding Dab2, and Runx1, which were previously shown to be induced by oncostatin-M (Osm) at the onset of CM dedifferentiation [13, 14]; accordingly, expression of the gene encoding Osm was also strongly increased, accompanied by a trend toward increased expression of the gene encoding its cognate receptor (Osmr). Other growth factor receptors that have been associated with CM dedifferentiation [15] were also increased in Tip60-depleted hearts, namely *Fgfr1* and *Tgfbr1*, as well as its ligand *Tgfb3* (Fig. 2b-c); however, *Fgf1*, which has not been previously reported in this context but which among members of the Fgf family is selectively expressed in CMs (per Tabula Muris [30]), was decreased (Figs. 2c, 4a).

Altered Expression of Genes indicative of EMT Transitioning & Cytoskeletal Disassembly in Tip60-depleted Hearts

Recent findings have indicated that CM proliferation is dependent on a dedifferentiation process in which CMs undergo a partial epithelial to mesenchymal-like transition (EMT-like; [16, 31]), accompanied by partial disassembly of the cytoskeleton/sarcomere complex ([32]; recently reviewed in [22]). We therefore assessed effects of Tip60 depletion on the expression of genes that regulate these processes. As shown in Figure 3a, >75% of the genes in the EMT GO Term were upregulated in infarcted/Tip60-depleted heart tissue, consistent with recently published findings showing that CM dedifferentiation induced by over-expression of Erbb2 is accompanied by the up-regulation of ~80% of 'EMT-like' genes [16]. Among the EMT-like genes up-regulated in the latter, 28 were also up-regulated in infarcted/Tip60-depleted hearts (Fig. 3b). In addition, as shown in Fig. 3c, we employed RT-qPCR to confirm up-regulation of the EMT genes *Gja1*, *Myocd*, *Myc*, and *Tbx20*, as well as the EMT-like genes *Actn1* which encodes α-Actinin and is normally expressed in developing CMs and in destabilized adult CMs [32], *Cttn* which encodes the actin-binding protein cortactin and promotes lamellipodia formation in migrating cells [33-35], and *Nes* which encodes the intermediate filament protein nestin in embryonic CMs [36] and was recently shown to be increased at the protein level in dedifferentiating CMs [16].

Among genes that have been associated with disassembly of the cytoskeleton, *Mapt* was of considerable interest because it not only encodes Tau protein, which maintains microtubule stability, but also because its expression during neurogenic reprogramming is highly dependent on Tip60 [24]. As expected, RNAseq revealed that expression of *Mapt*, which among cells in the heart is modestly but selectively expressed in CMs per Tabula Muris [30], was ~50% reduced in Tip60-depleted hearts (Fig. 3d). Other cytoskeletal genes depressed in Tip60-depleted hearts included *Mylk4*, which encodes a CM-specific kinase that maintains the myofilament skeleton [37, 38], *Myom1* (myomesin-1), a CM dedifferentiation marker [13, 39] that maintains the thick filament, and *Acta2* (smooth muscle actin), which has been reported to be decreased [16], as well as increased [13, 15], during CM dedifferentiation. Regarding *Acta2*, these disparate effects of dedifferentiation may be reconciled because decreased expression was detected by RT-qPCR and RNAseq performed on tissue samples from intact hearts (Fig. 3b-d and ref. [16]), whereas increased expression was observed by western blotting isolated CMs, and in CMs within immunostained hearts [13, 15]. The latter is consistent with our immunostaining observations indicating that α-sma is upregulated in CMs within the border zone of infarcted/Tip60-depleted hearts (Supp. Fig. 7). Taken together, these findings suggest the possibility that *Acta2* down-regulation reflects its reduced expression within, or reduced invasion of, myofibroblasts in the dedifferentiating heart, a possibility consistent with reduced scarring that we have observed in infarcted/Tip60-depleted hearts [10, 11]; we are following-up this possibility. Regarding up-regulated markers, it is noteworthy that *Cdk1*, which may regulate sarcomere disassembly [32], exhibited a trend toward marked increase, and that *Shroom 3*, which regulates polarity, cytoskeletal organization, and proliferation in developing CMs [40], was significantly up-regulated in infarcted/Tip60-depleted hearts (Fig. 3c-d). Finally, relative expression of the sarcomeric genes encoding the embryonic (*Tnni1*) and adult (*Tnni3*) isoforms of troponin I, which is considered to denote a molecular signature indicative of CM maturation [41, 42], was strongly re-directed toward the immature/dedifferentiated state in infarcted hearts that were depleted of Tip60 (Fig.3c-d).

Increased Expression of 'Soft' ECM Genes in Infarcted/Tip60-depleted Hearts

As the heart develops, proteomic analysis has shown that the extracellular matrix (ECM) undergoes substantial change, from softness to rigidity, as indicated by the relative abundance of collagen 4, emilin-1, fibronectin and periostin at immature stages, which transitions to high levels of collagen-1, collagen-3 and laminin by adult stages [19]. Retention of ECM softness has been shown to maintain CM proliferation in the neonatal heart [17]. To enable CM proliferation in the adult heart, findings in zebrafish [43, 44] and mouse [45] models indicate that CMs must be able to migrate, requiring a matrix metalloproteinase-induced transition from rigid to soft ECM. Based on these findings it was of interest to assess whether depletion of Tip60 promoted the expression of genes associated with matrix softening and cell migration. Consistent with ECM softening, Figure 4 shows that depletion of Tip60 beginning three days post-MI was followed eleven days later by increased expression of most genes in the GO Term 'Extracellular Matrix' (Fig. 4a), as well as increased expression of the genes shown in Figure 4b (verified by RT-qPCR; Fig. 4c), which have been associated with soft, immature ECM: *Col4a1, Col4a2, Emilin1*, *Fn1*, and *Postn;* the latter, periostin, which was increased >8-fold, has been shown to promote CM proliferation and cardiac

repair [46]. Also included among ECM genes exhibiting increased expression were those associated with Erbb2-induced CM dedifferentiation [31], including *Fn1*, *Loxl2, Col3a1*, *Col4a2*, *Col6a1*, *Col8a2*, and *Col15a1,* the latter of which is required for remodeling of the myocardial matrix and induction of CM proliferation [47-49]. Tip60 depletion was also accompanied by increased expression of ECM genes associated with Fgfr1/Osmr-induced dedifferentiation [15] -- *Col8a1*, *Emilin-1*, *Timp1*, and *Agrn* (agrin) – among which the latter has been shown to promote cardiac regeneration post-MI [18, 50]. The following genes reported to be increased in both Erbb2- [31] and Fgfr1/OsmR-induced [15] CMs were also increased in Tip60-depleted hearts: *Col1a1, Col4a1, Ctgf, Mmp2, Postn,* and *Vcan*, the latter of which supports cellular migration in the developing heart [51]. Finally, the most dramatically up-regulated ECM component in the Tip60-depleted heart was *Cthrc1* (>11-fold), which encodes collagen triple helix repeat containing 1 protein [52], and which is required for ECM reconstruction after injury in the developing [53] and adult heart [54]. In summary, findings in Figure 4 support the notion that depletion of Tip60 post-MI induces CM dedifferentiation, concomitant with matrix softening to effect CM migration/proliferation in the regenerating adult myocardium.

Altered Metabolic Programming in Infarcted/Tip60-depleted Hearts

Transition from neonatal to mature stages of cardiac development is accompanied by the metabolic transition from glycolysis to fatty acid oxidation (FAO) in CMs (review; [55]). Recent findings have shown that after MI, the ability of adult CMs to re-enter the cell-cycle requires dedifferentiation accompanied by metabolic reprogramming toward resumption of glycolysis [15, 16, 56, 57]. Hence it was of interest to assess the effects of depleting Tip60 post-MI on the expression of genes that regulate fatty acid oxidation (Fig. 5), TCA cycle (Fig. 6), and glycolysis (Fig. 7). As shown in Figure 5a, although Cre-recombinase alone (*Kat5*$^{+/+;merCremer}$) affected the expression of some genes within the GO Term 'Fatty Acid β-Oxidation' (FAO), nearly all were strongly down-regulated in hearts in which the *Kat5* gene was ablated (*Kat5*$^{\Delta/\Delta}$). Down-regulated genes included the battery regulating breakdown of short-chain thru very long-chain fatty acids (*Acads, Acadm, Acadl, Acadvl*), all of which are robustly expressed in the heart (Fig. 5b). It was particularly noteworthy that expression of carnityl palmitoyltransferase 1B (*Cpt1b*), which governs the rate-limiting step in FAO, was significantly reduced in Tip60-depleted hearts, since its targeted depletion in CMs was recently reported to cause dedifferentiation and renewed CM proliferation [57]. Although increased levels of *Cpt1c* were seen, expression of this isoform in adult CMs is negligible [30].

Regarding Krebs Cycle genes, despite a downward trend caused by Cre-recombinase (Fig. 6a), Tip60 depletion was associated with the strongly reduced expression of gene families that regulate each step of the cycle (Fig. 6b). One notable exception was the gene encoding α-ketoglutarate dehydrogenase (*Ogdh*), which along with *Aco2* and *Mdh2* are the most robustly expressed TCA cycle genes in the heart. Regarding *Ogdh*, like *Cpt1b* its targeted disruption was recently reported to be associated with cell-cycle activation and increased numbers of CMs [57].

Based on the reduced expression of most genes that regulate Fatty Acid β-Oxidation (Fig. 5) and the TCA Cycle (Fig. 6), it was anticipated that a reversion toward glycolysis would be observed in infarcted/Tip60-depleted hearts. Although genes governing crucial glycolytic steps, including *Hk1* which encodes the rate-limiting enzyme hexokinase-1, were up-regulated, it was surprising that most genes within the glycolytic GO term were decreased (Fig. 7a). However as discussed below, isoforms in glycolytic gene families that are relatively weakly expressed in the heart, including *Slc2a1*, *Slc16a3*, *Slc16a7*, *Pfkl*, *Eno1*, *Eno2*, *Pdk3*, *Ldha*, were significantly up-regulated in Tip60-depleted hearts (Fig. 7b-c).

To emphasize potential clinical relevance of depleting Tip60, the data described in Figures 2-7 address the effect of depleting Tip60 post-MI. To compare with effects of inhibiting Tip60 in the non-injured environment, RNA-seq was also performed on naïve, non-injured hearts that were Tip60-depleted. Figure 8 compares GO terms containing DEGs in non-injured versus infarcted hearts that were Tip60-depleted. Among the top 25 GO terms that were up-regulated after depleting Tip60, only those regulating cilium organization and cellular projection were increased in both the naïve and injured myocardial environments (Fig. 8a-b). Remarkably, whereas most of the up-regulated DEGs in the Tip60-depleted naïve (i.e., 11 dpt) myocardium were those regulating nucleic acid processing (Fig. 8a), most of the top 25 DEGs in infarcted/Tip60-depleted (i.e., 14 dpi) hearts were in GO terms associated with cell cycling, adhesion, and migration, and ECM organization (Fig. 8b). By contrast, the top 25

GO terms that were down-regulated in naïve and infarcted Tip60-depleted hearts were similar. Among these it is noteworthy that nearly half – including lipid metabolic process, TCA cycle, mitochondrial respiratory chain complex/mitochondrial organization, and oxidation-reduction process – were associated with metabolic alterations (Fig. 8c-d). Taken together, these results imply that, in addition to strongly promoting CM dedifferentiation, inhibition of Tip60 in the infarcted myocardial environment promotes re-activation of the CM cell-cycle, conditions that favor cardiac regeneration. Finally, as discussed below it is noteworthy that the genes within the GO term '2-oxoglutarate metabolic process' were down-regulated in infarcted/Tip60-depleted hearts (Fig. 8d).

Reduced Levels of Trimethylated Histone H3 (H3K4me3) in Tip60-depleted Hearts

Coincident with their finding that Tip60-mediated acetylation of histone H2A.Z is required to reprogram murine embryonic fibroblasts into neurons, Janas et al.[58] showed that Tip60 promotes the deposition of methylated histone H3 ($H3K4^{me3}$) into promoters of genes that induce lineage specification, creating a bivalent activational mark. It was therefore of interest to assess whether Tip60 depletion affects levels $H3K4^{me3}$ in CM nuclei. Based on immunostaining shown in Figure 9, levels of $H3K4^{me3}$ are modestly but significantly reduced in Tip60-depleted nuclei, in accord with the idea that Tip60, perhaps via its chromodomain, recruits $H3K4^{me3}$ to genes that confer cardiomyocyte maturity.

DISCUSSION

Resume: Recent findings in this laboratory have supported the hypothesis that genetic depletion [10, 11] or pharmaceutical inhibition [12] of the pleiotropic acetyltransferase Tip60 (*Kat5*) confers cardioprotection and regeneration after myocardial infarction (MI) by preventing the site-specific acetylation and activation of targets that are pro-apoptotic (i.e., p53) and anti-proliferative (i.e., Atm). Here we report findings showing that depletion of Tip60 post-MI extinguishes acetylation of the histone variant H2A.Z in CMs, a chromatin target associated with induction and maintenance of the differentiated state in other cell types; we accordingly also show that reduced acetylation of H2A.Z is associated with CM dedifferentiation, a status considered pre-requisite for the ability of CMs to undergo cell-cycle reactivation and bona fide proliferation to effect myocardial regeneration [13-17, 22, 59-61]. Specifically, western blotting (Fig. 1b) indicated that depletion of Tip60 post-MI reduced levels of H2A.Zac$^{K4/K7}$ in heart tissue by approximately two-thirds (Fig. 1b). Most remarkably, immunostaining revealed near-complete obliteration of H2A.Zac$^{K4/K7}$ in CM nuclei of naïve hearts and in the remote zone of infarcted hearts (Fig. 1a); we speculate that retention of H2A.Zac$^{K4/K7}$ in ~30% of CM nuclei within the border zone may reflect inability of tamoxifen to perfuse this region due to vascular injury, and/or possibly due to increased Tip60 protein levels in infarcted tissue that we observed in preliminary findings. In combination with RNAseq data (Figs. 2-7) indicating CM dedifferentiation in Tip60-depleted CMs, our findings are consistent with earlier reports that (i) H2A.Z acetylation is required for skeletal [62] and smooth [63] muscle cell differentiation, (ii) more recently that acetylation of H2A.Z by Tip60 is required to maintain hematopoietic stem cell differentiation [23], and (iii) most recently that site-specific acetylation of H2A.Z by Tip60 is required for neuronal differentiation [24]. Because the latter reports demonstrated that acetylated H2A.Z binds pioneer transcription factors that activate genes to establish cellular maturity – specifically Myc in HSCs [23] and Ascl1 in neurons [24] – it will be of extraordinary interest to ascertain whether H2A.Zac$^{K4/K7}$ recruits the pioneer cardiomyogenic transcription factors to enhancer/promoter loci in genes that maintain the CM differentiated state.

Extracellular Matrix: Alterations in the extracellular matrix during cardiac development and after injury, which are dependent upon crosstalk between CMs and fibroblast sub-populations in the myocardium, are the subject of a recent outstanding review [64]. As discussed above in Figure 4, many of the ECM genes exhibiting increased expression after depleting Tip60 post-MI have previously been associated with transition toward a relatively soft neonatal-like matrix within which CMs can migrate and proliferate [15-17]. However, questions remain as to why mature ECM genes associated with stiffening and scar formation, especially those encoding fibrillar collagens (types 1 and 3) as well as members of the lysyl oxidase family (*Lox*, *Loxl2*) which regulate collagen cross-linking, were also robustly up regulated when Tip60 is depleted. In this regard, *Col1a1* and *Lox*, the latter of which has also been associated with soft matrix construction, were previously associated with CM dedifferentiation [15]. An interesting possibility to consider is that matrix softening is enhanced by the >11-fold increase in *Cthrc1* -- perhaps the most differentially expressed gene in our dataset -- encoding collagen triple helix repeat containing-1 protein, that not only has a crucial role in wound healing [54], but has also been shown to limit the deposition of collagen matrix during arterial remodeling [65, 66] and promote cellular migration [67]. An additional question regards how the ECM gene battery, expression of which is essentially specific to various fibroblast subpopulations in the myocardium [54], transitions toward softness when Tip60 is depleted in CMs; while the transition toward soft ECM is likely regulated via crosstalk between the Wnt/β-catenin, Hippo/Yap and TGFβ pathways [64], mechanistic details of signaling between these various cell types remains speculative.

Metabolic Reprogramming: Effects of Tip60 depletion on the expression of metabolic genes was largely consistent with emerging dogma that CM dedifferentiation is accompanied by metabolic reprogramming (Figs. 5-7), wherein fatty acid oxidation (FAO) reverts to glycolysis (review, [68]). Most prominently, Tip60 depletion was associated with reduced expression of genes that regulate fatty acid oxidation (Fig. 5) and key steps in the TCA cycle (Fig. 6). While evidence of renewed glycolysis was less dramatic (Fig. 7a), previous findings showing that reversion to glycolysis during CM dedifferentiation is accompanied by increased expression of genes encoding pyruvate dehydrogenase kinase 3 (*Pdk3*), monocarboxylate transporter 3 (*Slc16a3;* Mct4) [16], and glucose transporter 1 (*Slc2a1*; Glut1) [56] were recapitulated by Tip60 depletion (Fig. 7b-c). Interestingly, although the most robustly expressed glucose transporter, *Slc2a4* (Glut4) was markedly depressed after Tip60 depletion, expression of *Slc2a1*, a relatively weakly expressed isoform, was upregulated (Fig. 7b-c); in this regard it is relevant

that over-expression of *Slc2a1* has been shown to mitigate heart failure [69], and was recently associated with cardiac regeneration [70, 71]. Depletion of Tip60 after infarction was also associated with the significantly increased expression of isoforms in other glycolysis gene families (*Slc16a7*, *Pfkl*, *Eno1*, *Eno2, Ldha;* Fig. 7b-c) that are normally weakly expressed in the heart. This suggests the interesting possibility that because the dedifferentiation process reduces expression of 'mature' isoforms that are robustly expressed in CMs, reversion to glycolysis is mediated by the increased expression of isoforms that are normally weakly expressed in the adult heart. To assess whether increased expression of hexokinase, along with weakly-expressed glycolytic isoforms, is sufficient to maintain respiration in infarcted/Tip60-depleted hearts, we are performing Seahorse assays on CMs isolated from infarcted/Tip60-depleted hearts.

Effect on CM Proliferation: Our previous findings that Tip60 depletion post-MI maintains cardiac function, diminishes fibrosis and activates the CM cell-cycle [10, 11], as well as the findings reported here that depletion also induces a dedifferentiated state permissive for CM proliferation, are consistent with the notion that targeting Tip60 efficiently permits heart regeneration post-MI. However it remains unsettled whether bona fide proliferation of CMs ensues, expanding numbers of CMs that are mononuclear and diploid, which are considered reparative. Per our recent review [72], resolution of this seemingly straightforward question has been forestalled by the absence of reliable methodologies capable of ensuring that mononuclear cells positive for BrdU, Ki67 and H3P in the *in vivo* heart are indeed CMs, and are not polyploid. Using a recently developed method that enables unequivocal assessment of cellular identity, ploidy and nuclearity in CMs dis-aggregated from the heart [73, 74], we are addressing this question in depth. Should this reveal that numbers of reparative CMs are static or only marginally increased, we will employ measures to further drive proliferation by more extensively depleting Tip60.

Epigenetic Maintenance of the Differentiated State: It was recently reported [57] that depletion of *Cpt1b* in CMs causes accumulation of the Krebs cycle metabolite α-ketoglutarate (αKG), which by co-activating lysine demethylase 5 (Kdm5) depletes levels of histone H3K4^{me3} in chromatin encoding CM 'maturity' genes, resulting in CM dedifferentiation and cell-cycle activation. While our RNAseq data suggest that Tip60 depletion would not reduce H3K4^{me3} levels, since expression of isocitrate dehydrogenase (*Idh*) (which generates αKG) is reduced (Figs. 6 & 8) and expression of α-ketoglutarate dehydrogenase (which catabolizes αKG) is not inhibited (Fig. 6), immunostaining of H3K4^{me3} in Tip60-depleted hearts indicated that levels are modestly but significantly depleted. Reduction of H3K4^{me3} is consistent with findings during neuronal reprogramming that depletion of Tip60, the chromodomain of which binds trimethylated lysines in histone H3 [75-77], prevents the deposition of H3K4^{me3} into 'maturity' genes that encode neuron-specific proteins. Findings that H3K4^{me3} levels are required to maintain the differentiated state in CMs [57], combined with findings reported here associating deacetylated H2A.Zac$^{K4/K7}$ with dedifferentiation, may be indicative of an epigenetic topography that regulates the differentiated state in CMs, and ultimately their ability to divide.

Conclusions: The findings reported here indicating that genetic depletion of Tip60 nearly completely extinguishes acetylation of H2A.Zac$^{K4/K7}$ in CM nuclei while inducing CM dedifferentiation, considered with our previous findings that Tip60 depletion in CMs beginning three days post-MI promotes CM cell-cycle activation, reduces apoptosis and scarring, and preserves cardiac function [10, 11] -- effects that are mimicked using drugs that inhibit Tip60's acetyltransferase (AT) domain (TH1834 in ref [12]; pentamidine in an 'in preparation' manuscript) -- warrant pharmaceutical targeting of this pleiotropic factor to ameliorate cardiac injury. Toward this end we are developing drugs that target Tip60's chromodomain because this moiety, which reportedly binds H3K4^{me3} [75, 76], unlike the AT domain is unique with the ~20-member acetyltransferase family.

Limitations of these Findings: Although we attempted to avoid off-target effects of cre-recombinase by withholding determinations until a minimum of nine days had transpired following the first of three tamoxifen injections (i.e, 14 days post-MI), by which time our previous work indicated that off-target effects in CMs are subsided [78], and although only ~75 genes were mis-expressed in identically treated wild-type controls expressing the *Myh6-merCremer transgene* (Supp. Fig. 1b), possible effects were observed, especially among the metabolic GO terms in Figures 5-7.

FIGURES & LEGENDS

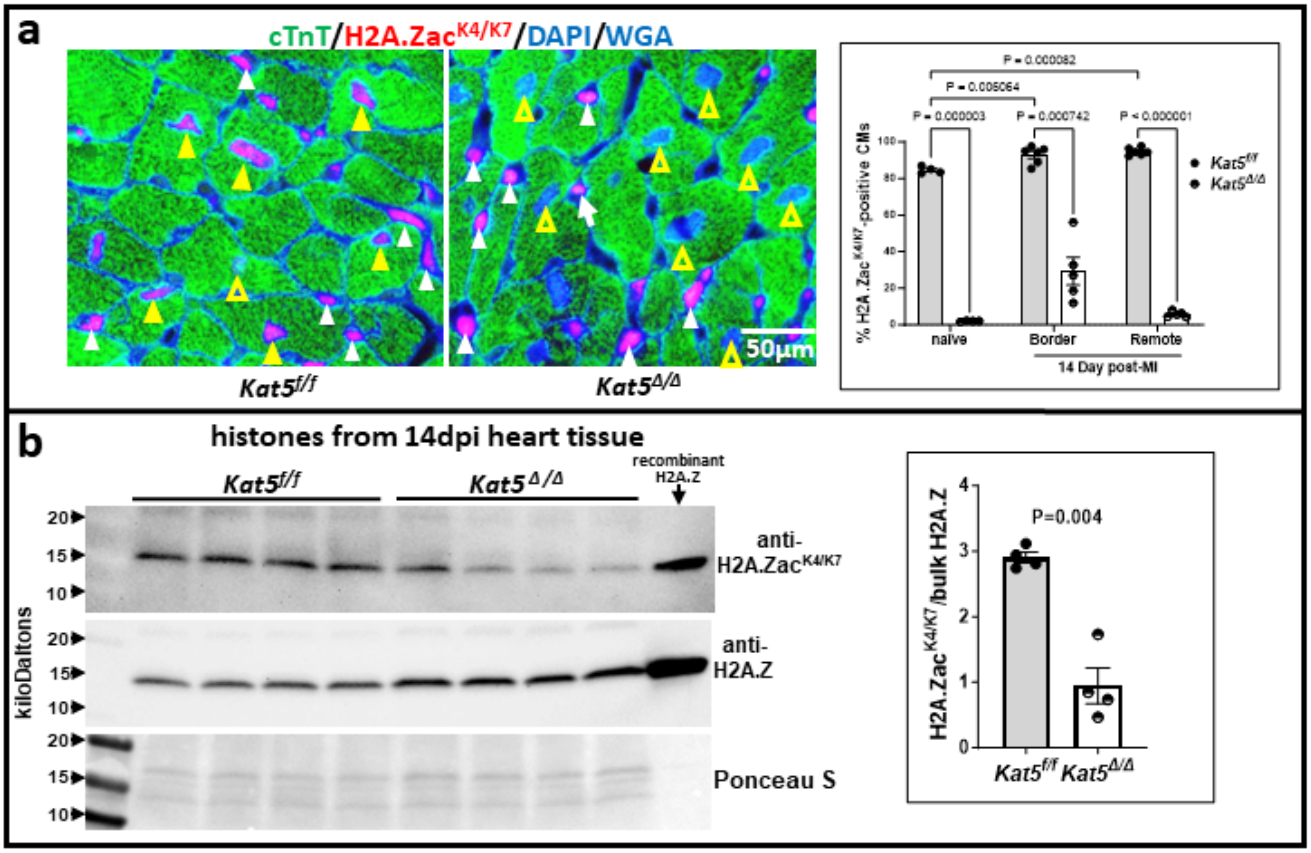

Fig. 1. Depletion of histone H2A.Z acetylation in Tip60-depleted CMs. **Panels a** & **b** respectively show representative images of control (*Kat5*$^{f/f}$) and experimental (*Kat5*$^{\Delta/\Delta}$) adult hearts wherein Tip60 was depleted from the latter by injecting tamoxifen for three consecutive days beginning on the third day after myocardial infarction (MI). Hearts were removed for processing on day 14 post-MI.
a, Immunostain: In control hearts (*Kat5*$^{f/f}$), acetylated H2A.Z (H2A.Zac; red fluorescence) is present in nuclei of most non-CMs (white arrowheads) and CMs (filled yellow arrowheads). In Tip60-depleted hearts (*Kat5*$^{\Delta/\Delta}$), H2A.Zac is present in non-CM nuclei (white arrowheads) but is conspicuously absent in most CM nuclei (open yellow arrowheads). At right, percentages of cell-cycle-activated CMs were enumerated by blinded observers.
b, Western blots showing acetylated (above) vs. non-acetylated (i.e., bulk, middle) H2A.Z protein in heart tissue. Right, densitometry showing altered levels of H2A.Zac normalized to bulk H2A.Z.
In **panels a & b**, *P<0.05 vs. *Kat5*$^{f/f}$ per unpaired Student's t-test; means ±SEM. Each point represents a biological replicate (i.e., an individual mouse heart).

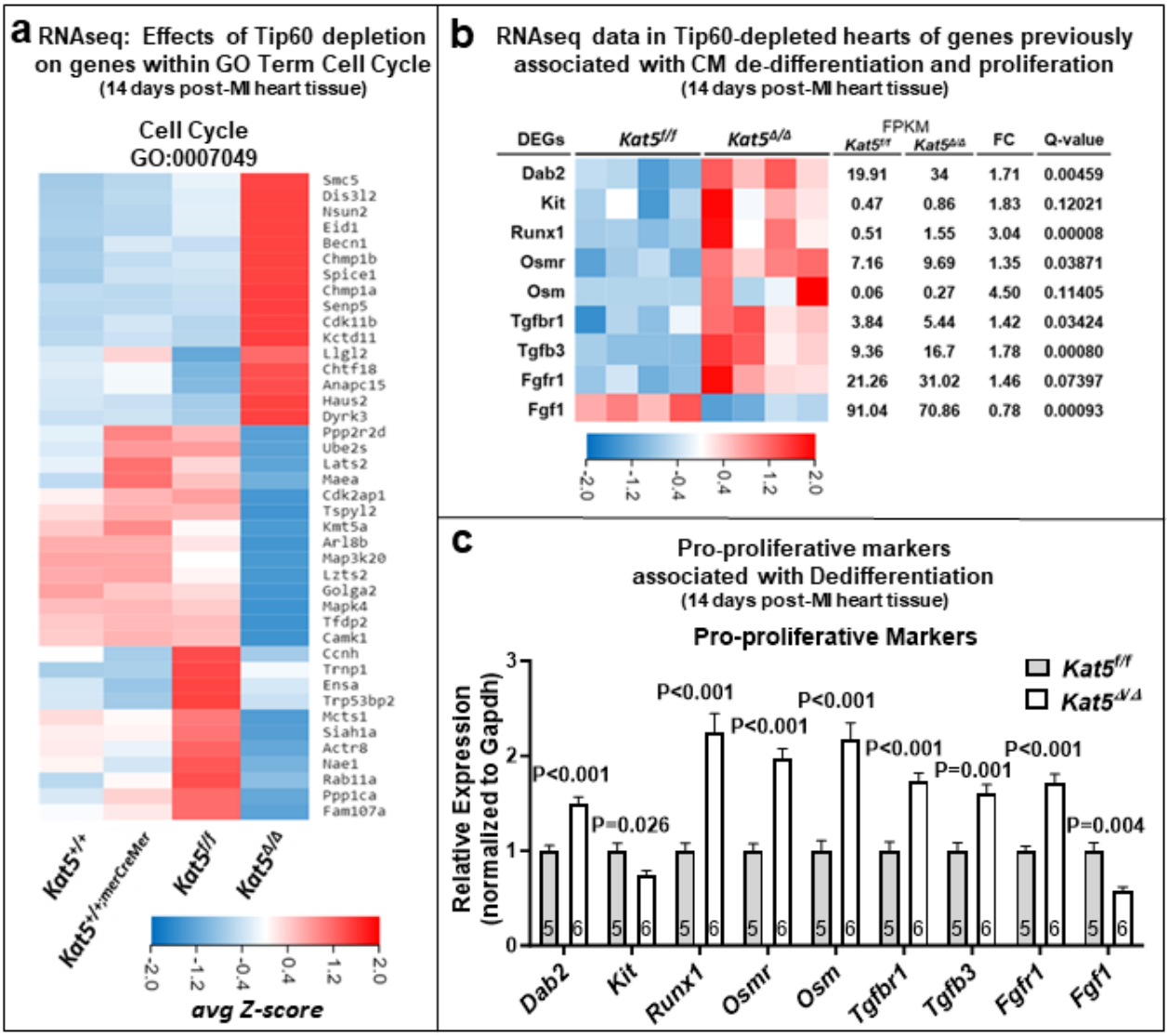

Figure 2. Expression of genes associated with proliferative signaling during CM dedifferentiation in infarcted/Tip60-depleted hearts at 14 days post-MI. Panel a: RNAseq data showing altered gene expressions within the Gene Ontology Cell Cycle term. *Kat5*$^{f/f}$ = control, *Kat5*$^{\Delta/\Delta}$ = Tip60-depleted; *Kat5*$^{+/+}$ and *Kat5*$^{+/+;merCremer}$ were compared to assess off-target effects of Cre-recombinase. **Panels b & c:** Respective RNAseq and RT-qPCR data for genes associated with proliferative signaling during CM dedifferentiation. In **b**, each colored column represents a biological replicate. In **c**, each biological replicate (N; shown inside bar) is from a single heart; each was subjected to three technical replicates. Data are Mean ±SEM, compared by unpaired, two-tailed Student's t tests with Welch's correction.

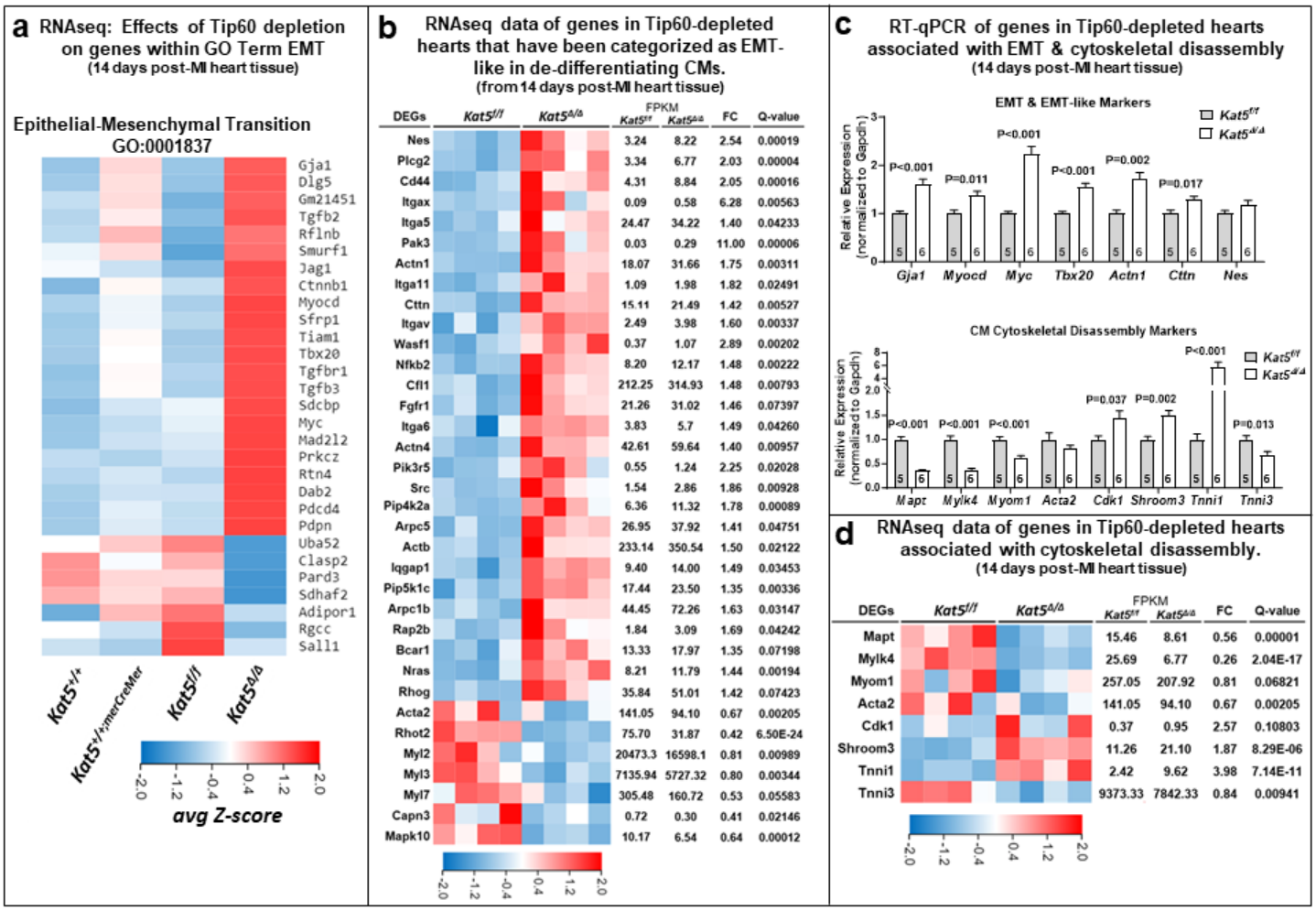

Figure 3. Expression of genes associated with the epithelial-mesenchymal transition (EMT) & cytoskeletal stability in infarcted/Tip60-depleted hearts. Panel a: RNAseq results showing altered gene expression in the Gene Ontology term Epithelial Mesenchymal Transition (EMT). **Panel b:** RNAseq data of mis-expressed EMT-like genes in infarcted/Tip60-depleted hearts. **Panel c:** RT-qPCR data showing mis-expression of genes regulating EMT, EMT-like and Cytoskeletal processes in infarcted/Tip60-depleted hearts. **Panel d:** RNAseq data of mis-expressed genes involved in the regulation of cytoskeletal structure. *Kat5*$^{f/f}$ = control, *Kat5*$^{\Delta/\Delta}$ = Tip60-depleted. In **panel a**, *Kat5*$^{+/+}$ and *Kat5*$^{+/+;merCremer}$ were compared to assess off-target effects of Cre-recombinase. In **panel b**, each colored column represents a biological replicate. In **panel c**, each biological replicate (N; shown inside bar) is from a single heart; each was subjected to three technical replicates. All data are Mean ±SEM, compared by unpaired, two-tailed Student's t tests with Welch's correction.

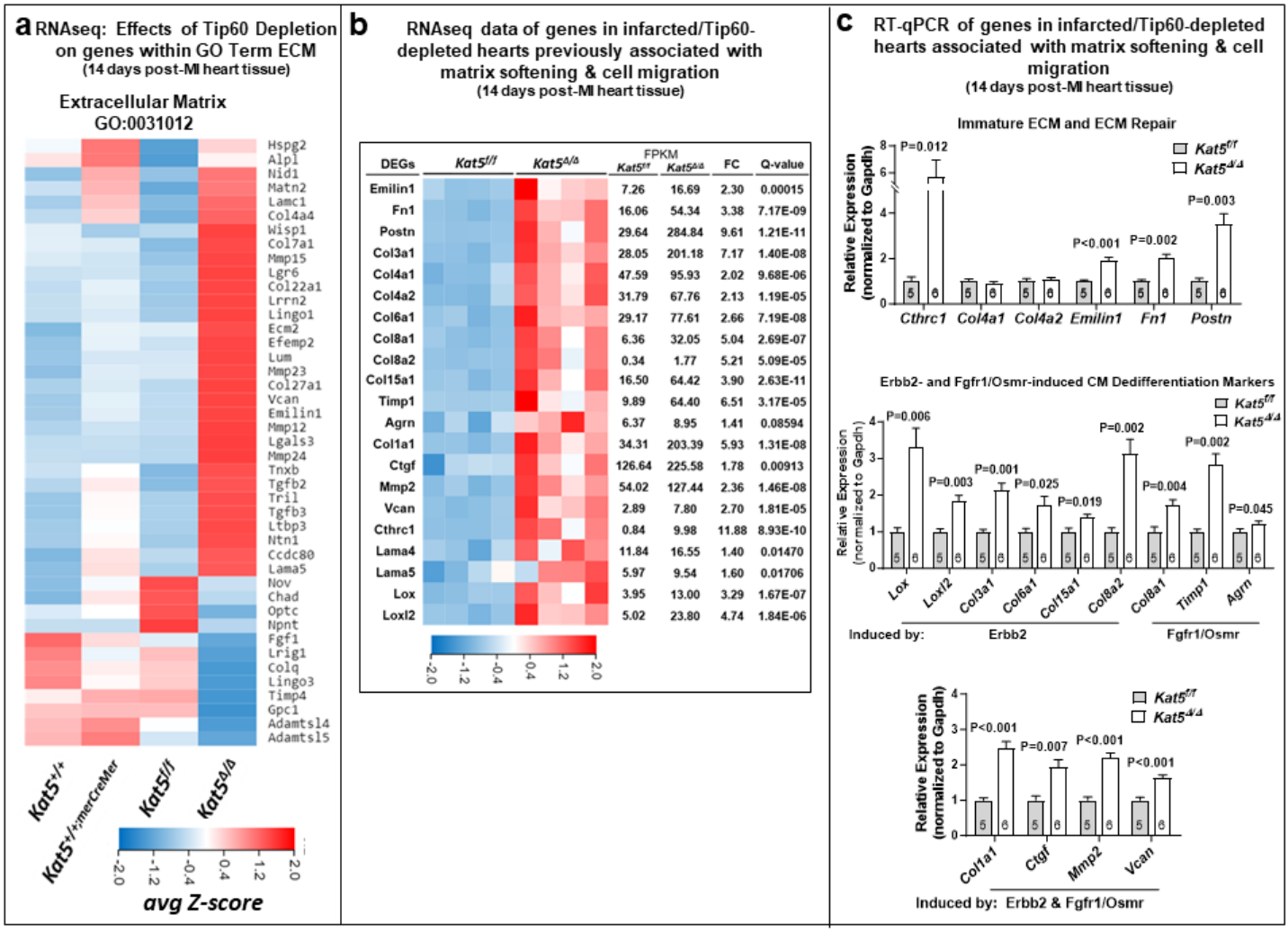

Figure 4. Expression of factors associated with transition to soft connective tissue and cell migration in infarcted/Tip60-depleted hearts at 14 days post-infarction. Panel a: RNAseq results showing gene mis-expressions in the GO term Extracellular Matrix (ECM). **Panel b:** RNAseq data of mis-expressed ECM genes in infarcted/Tip60-depleted hearts at 14 days post-MI. **Panel c:** RT-qPCR data showing mis-expression of genes regulating ECM components in infarcted/Tip60-depleted hearts. *Kat5*$^{f/f}$ = control, *Kat5*$^{\Delta/\Delta}$ = Tip60-depleted. In **panel a**, *Kat5*$^{+/+}$ and *Kat5*$^{+/+;merCremer}$ were compared to assess off-target effects of Cre-recombinase. In **panel b**, each colored column represents a biological replicate. In **panel c**, each biological replicate (N; shown inside bar) is from a single heart; each was subjected to three technical replicates. All data are Mean ±SEM, compared by unpaired, two-tailed Student's t tests with Welch's correction.

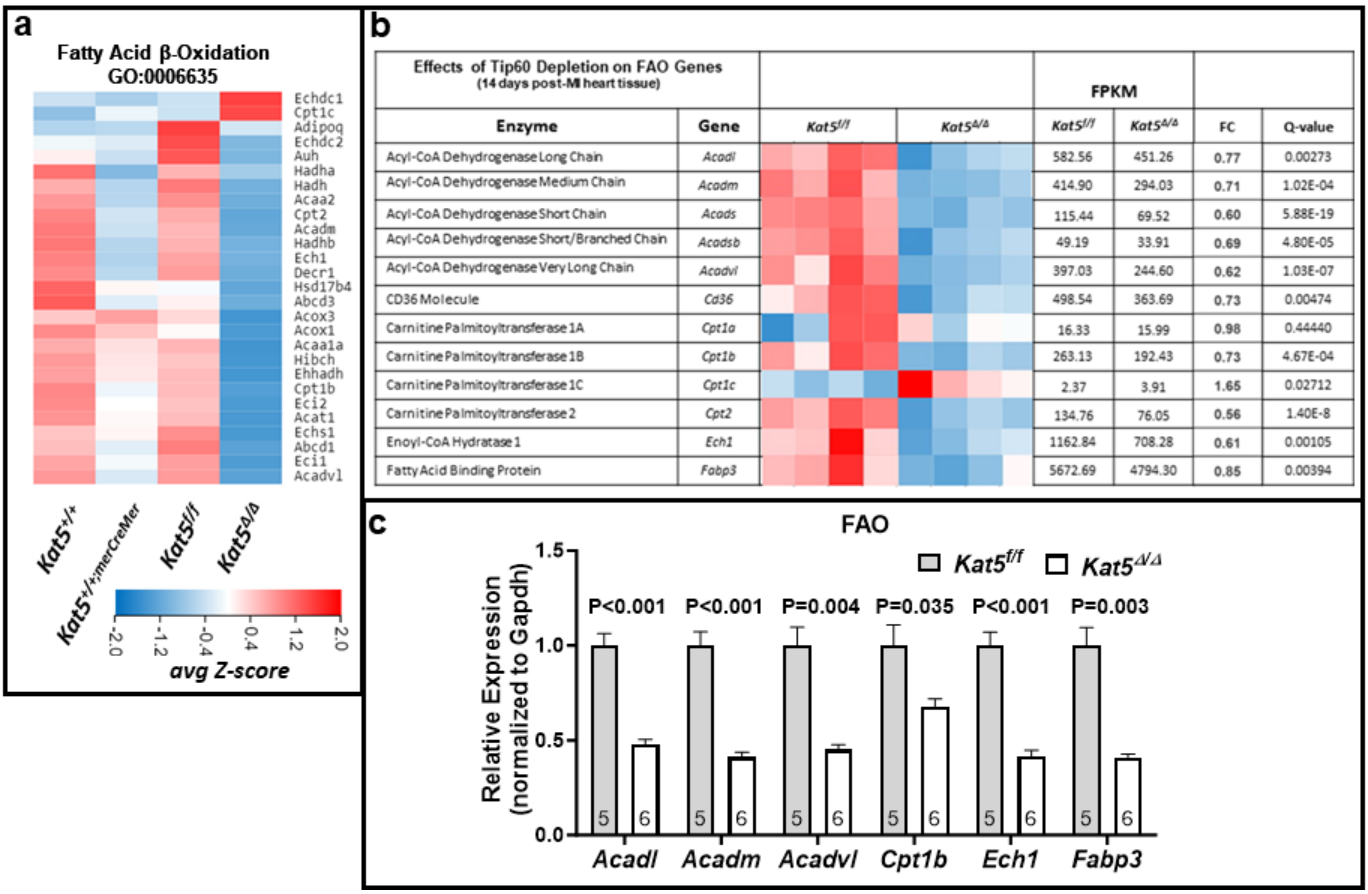

Effects of Tip60 Depletion on FAO Genes (14 days post-MI heart tissue)				FPKM			
Enzyme	Gene	*Kat5*$^{f/f}$	*Kat5*$^{\Delta/\Delta}$	*Kat5*$^{f/f}$	*Kat5*$^{\Delta/\Delta}$	FC	Q-value
Acyl-CoA Dehydrogenase Long Chain	*Acadl*			582.56	451.26	0.77	0.00273
Acyl-CoA Dehydrogenase Medium Chain	*Acadm*			414.90	294.03	0.71	1.02E-04
Acyl-CoA Dehydrogenase Short Chain	*Acads*			115.44	69.52	0.60	5.88E-19
Acyl-CoA Dehydrogenase Short/Branched Chain	*Acadsb*			49.19	33.91	0.69	4.80E-05
Acyl-CoA Dehydrogenase Very Long Chain	*Acadvl*			397.03	244.60	0.62	1.03E-07
CD36 Molecule	*Cd36*			498.54	363.69	0.73	0.00474
Carnitine Palmitoyltransferase 1A	*Cpt1a*			16.33	15.99	0.98	0.44440
Carnitine Palmitoyltransferase 1B	*Cpt1b*			263.13	192.43	0.73	4.67E-04
Carnitine Palmitoyltransferase 1C	*Cpt1c*			2.37	3.91	1.65	0.02712
Carnitine Palmitoyltransferase 2	*Cpt2*			134.76	76.05	0.56	1.40E-8
Enoyl-CoA Hydratase 1	*Ech1*			1162.84	708.28	0.61	0.00105
Fatty Acid Binding Protein	*Fabp3*			5672.69	4794.30	0.85	0.00394

Figure 5. Expression of genes associated with fatty acid oxidation in infarcted/Tip60-depleted hearts at 14 days post-infarction. Panel a: RNAseq results showing gene mis-expressions in the GO term Fatty Acid β-Oxidation (FAO). *Kat5*$^{f/f}$ = control, *Kat5*$^{\Delta/\Delta}$ = Tip60-depleted. *Kat5*$^{+/+}$ and *Kat5*$^{+/+;merCremer}$ were compared to assess off-target effects of Cre-recombinase. **Panel b:** RNAseq data of mis-expressed key FAO enzymes in infarcted/Tip60-depleted hearts at 14 days post-MI. Each colored column represents a biological replicate. **Panel c:** RT-qPCR data showing mis-expression of selected genes that regulate FAO in infarcted/Tip60-depleted hearts. Each biological replicate (N; shown inside bar) is from a single heart; each was subjected to three technical replicates. Data are Mean ± SEM, compared by unpaired, two-tailed Student's t tests with Welch's correction.

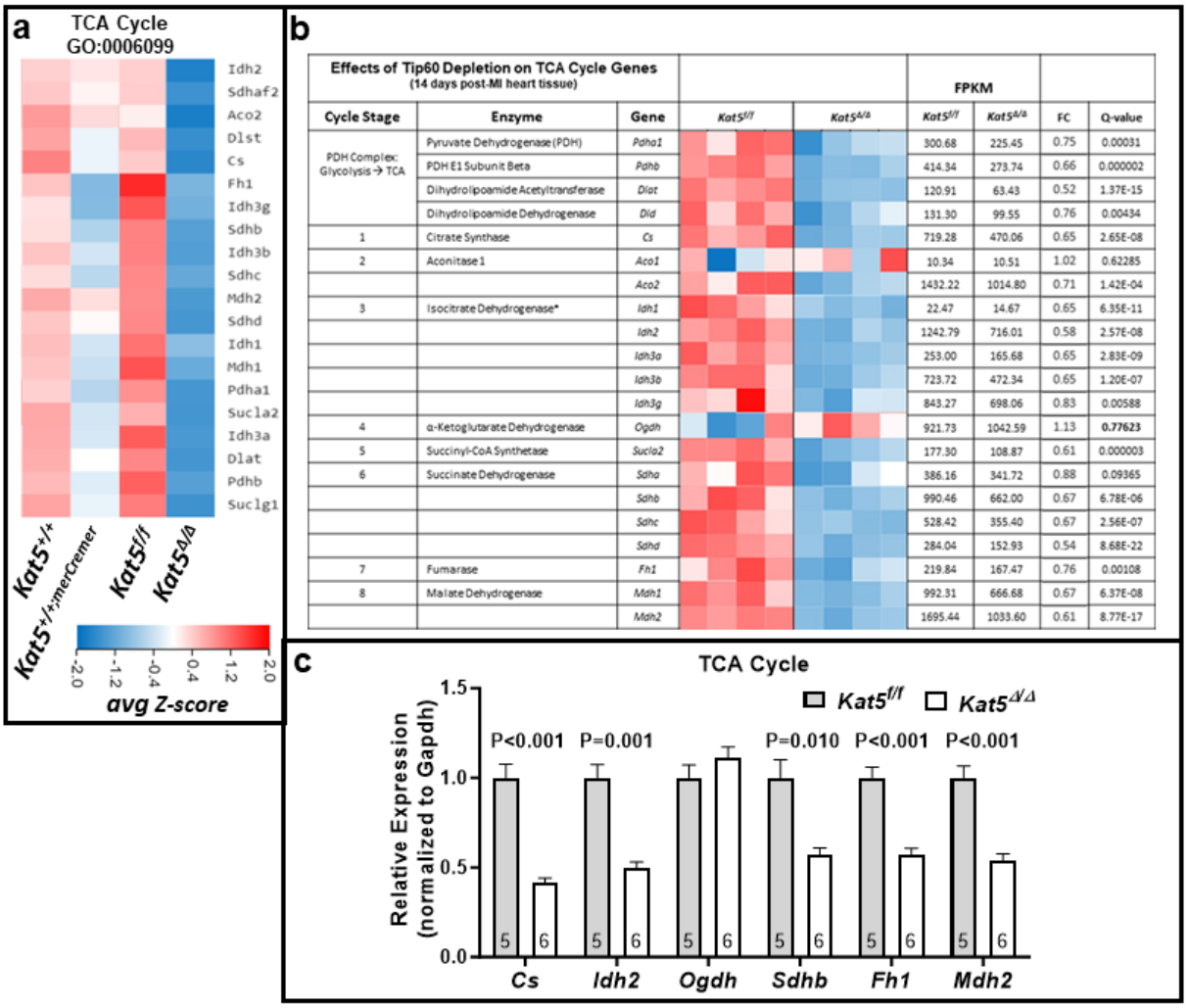

Effects of Tip60 Depletion on TCA Cycle Genes (14 days post-MI heart tissue)

Cycle Stage	Enzyme	Gene	FPKM $Kat5^{f/f}$	FPKM $Kat5^{\Delta/\Delta}$	FC	Q-value
PDH Complex: Glycolysis → TCA	Pyruvate Dehydrogenase (PDH)	*Pdha1*	300.68	225.45	0.75	0.00031
	PDH E1 Subunit Beta	*Pdhb*	414.34	273.74	0.66	0.000002
	Dihydrolipoamide Acetyltransferase	*Dlat*	120.91	63.43	0.52	1.37E-15
	Dihydrolipoamide Dehydrogenase	*Dld*	131.30	99.55	0.76	0.00434
1	Citrate Synthase	*Cs*	719.28	470.06	0.65	2.65E-08
2	Aconitase 1	*Aco1*	10.34	10.51	1.02	0.62285
		Aco2	1432.22	1014.80	0.71	1.42E-04
3	Isocitrate Dehydrogenase*	*Idh1*	22.47	14.67	0.65	6.35E-11
		Idh2	1242.79	716.01	0.58	2.57E-08
		Idh3a	253.00	165.68	0.65	2.83E-09
		Idh3b	723.72	472.34	0.65	1.20E-07
		Idh3g	843.27	698.06	0.83	0.00588
4	α-Ketoglutarate Dehydrogenase	*Ogdh*	921.73	1042.59	1.13	**0.77623**
5	Succinyl-CoA Synthetase	*Sucla2*	177.30	108.87	0.61	0.000003
6	Succinate Dehydrogenase	*Sdha*	386.16	341.72	0.88	0.09365
		Sdhb	990.46	662.00	0.67	6.78E-06
		Sdhc	528.42	355.40	0.67	2.56E-07
		Sdhd	284.04	152.93	0.54	8.68E-22
7	Fumarase	*Fh1*	219.84	167.47	0.76	0.00108
8	Malate Dehydrogenase	*Mdh1*	992.31	666.68	0.67	6.37E-08
		Mdh2	1695.44	1033.60	0.61	8.77E-17

Figure 6. Expression of genes associated with TCA cycle in infarcted/Tip60-depleted hearts at 14 days post-infarction. Panel a: RNAseq results showing gene mis-expressions in the GO term TCA cycle. *$Kat5^{f/f}$* = control, *$Kat5^{\Delta/\Delta}$* = Tip60-depleted. *$Kat5^{+/+}$* and *$Kat5^{+/+;merCremer}$* were compared to assess off-target effects of Cre-recombinase. **Panel b:** RNAseq data of mis-expressed enzymes that regulate each TCA cycle stage in infarcted/Tip60-depleted hearts at 14 days post-MI. Each colored column represents a biological replicate. **Panel c:** RT-qPCR data showing mis-expression of TCA cycle genes in infarcted/Tip60-depleted hearts. Each biological replicate (N; shown inside bar) is from a single heart; each was subjected to three technical replicates. Data are Mean ± SEM, compared by unpaired, two-tailed Student's t tests with Welch's correction.

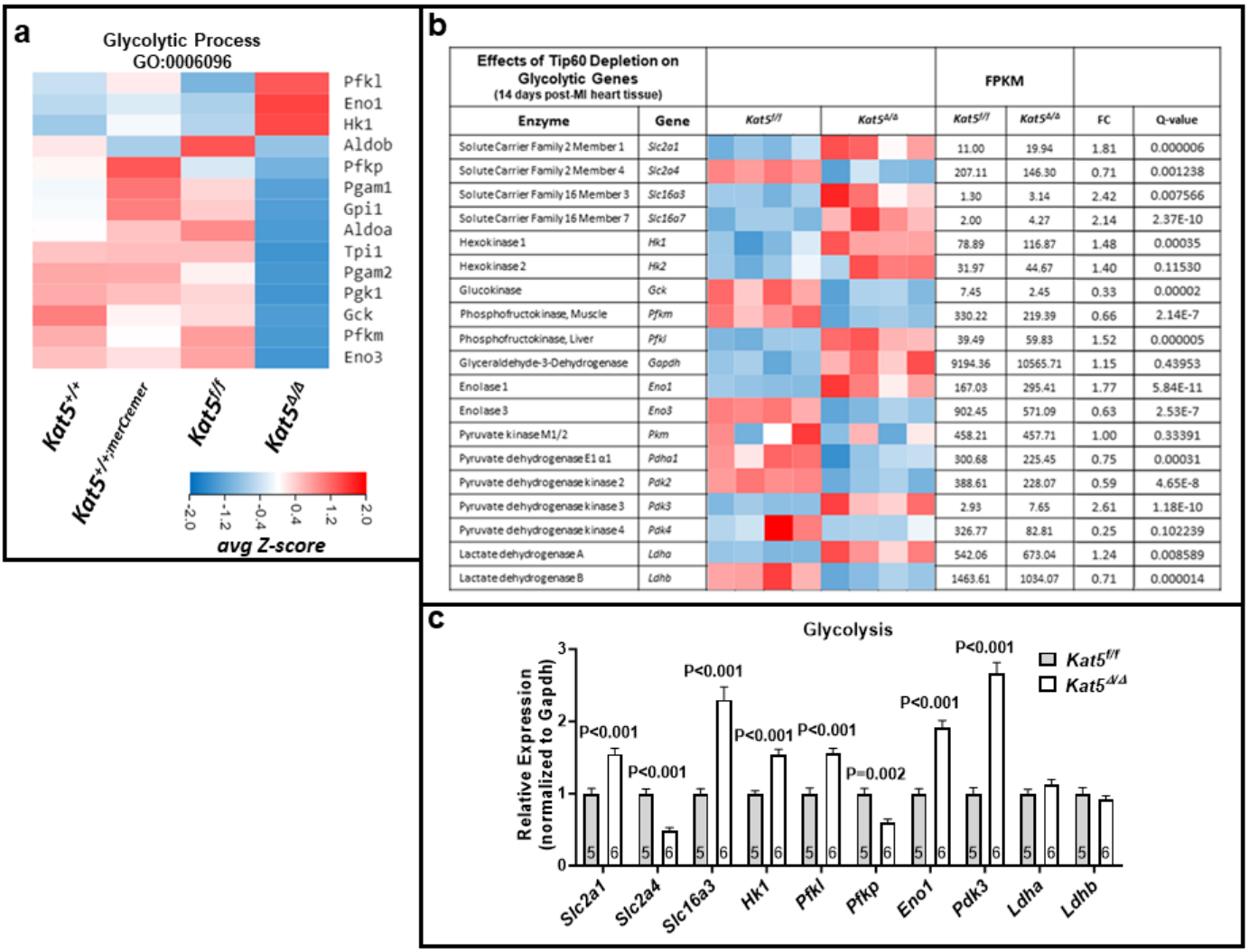

Effects of Tip60 Depletion on Glycolytic Genes (14 days post-MI heart tissue)				FPKM			
Enzyme	Gene	*Kat5f/f*	*Kat5Δ/Δ*	*Kat5f/f*	*Kat5Δ/Δ*	FC	Q-value
Solute Carrier Family 2 Member 1	*Slc2a1*			11.00	19.94	1.81	0.000006
Solute Carrier Family 2 Member 4	*Slc2a4*			207.11	146.30	0.71	0.001238
Solute Carrier Family 16 Member 3	*Slc16a3*			1.30	3.14	2.42	0.007566
Solute Carrier Family 16 Member 7	*Slc16a7*			2.00	4.27	2.14	2.37E-10
Hexokinase 1	*Hk1*			78.89	116.87	1.48	0.00035
Hexokinase 2	*Hk2*			31.97	44.67	1.40	0.11530
Glucokinase	*Gck*			7.45	2.45	0.33	0.00002
Phosphofructokinase, Muscle	*Pfkm*			330.22	219.39	0.66	2.14E-7
Phosphofructokinase, Liver	*Pfkl*			39.49	59.83	1.52	0.000005
Glyceraldehyde-3-Dehydrogenase	*Gapdh*			9194.36	10565.71	1.15	0.43953
Enolase 1	*Eno1*			167.03	295.41	1.77	5.84E-11
Enolase 3	*Eno3*			902.45	571.09	0.63	2.53E-7
Pyruvate kinase M1/2	*Pkm*			458.21	457.71	1.00	0.33391
Pyruvate dehydrogenase E1 α1	*Pdha1*			300.68	225.45	0.75	0.00031
Pyruvate dehydrogenase kinase 2	*Pdk2*			388.61	228.07	0.59	4.65E-8
Pyruvate dehydrogenase kinase 3	*Pdk3*			2.93	7.65	2.61	1.18E-10
Pyruvate dehydrogenase kinase 4	*Pdk4*			326.77	82.81	0.25	0.102239
Lactate dehydrogenase A	*Ldha*			542.06	673.04	1.24	0.008589
Lactate dehydrogenase B	*Ldhb*			1463.61	1034.07	0.71	0.000014

Figure 7. Expression of genes associated with glycolysis in infarcted/Tip60-depleted hearts at 14 days post-infarction. Panel a: RNAseq results showing gene mis-expressions in the GO term Glycolytic Process. *Kat5*$^{f/f}$ = control, *Kat5*$^{\Delta/\Delta}$ = Tip60-depleted. *Kat5*$^{+/+}$ and *Kat5*$^{+/+;merCremer}$ were compared to assess off-target effects of Cre-recombinase. **Panel b:** RNAseq data of mis-expressed genes that regulate glycolytic steps in infarcted/Tip60-depleted hearts at 14 days post-MI. Each colored column represents a biological replicate. **Panel c:** RT-qPCR data showing altered expression of the glycolytic process gene isoforms in infarcted/Tip60-depleted hearts. Each biological replicate (N; shown inside bar) is from a single heart; each was subjected to three technical replicates. Data are Mean ± SEM, compared by unpaired, two-tailed Student's t tests with Welch's correction.

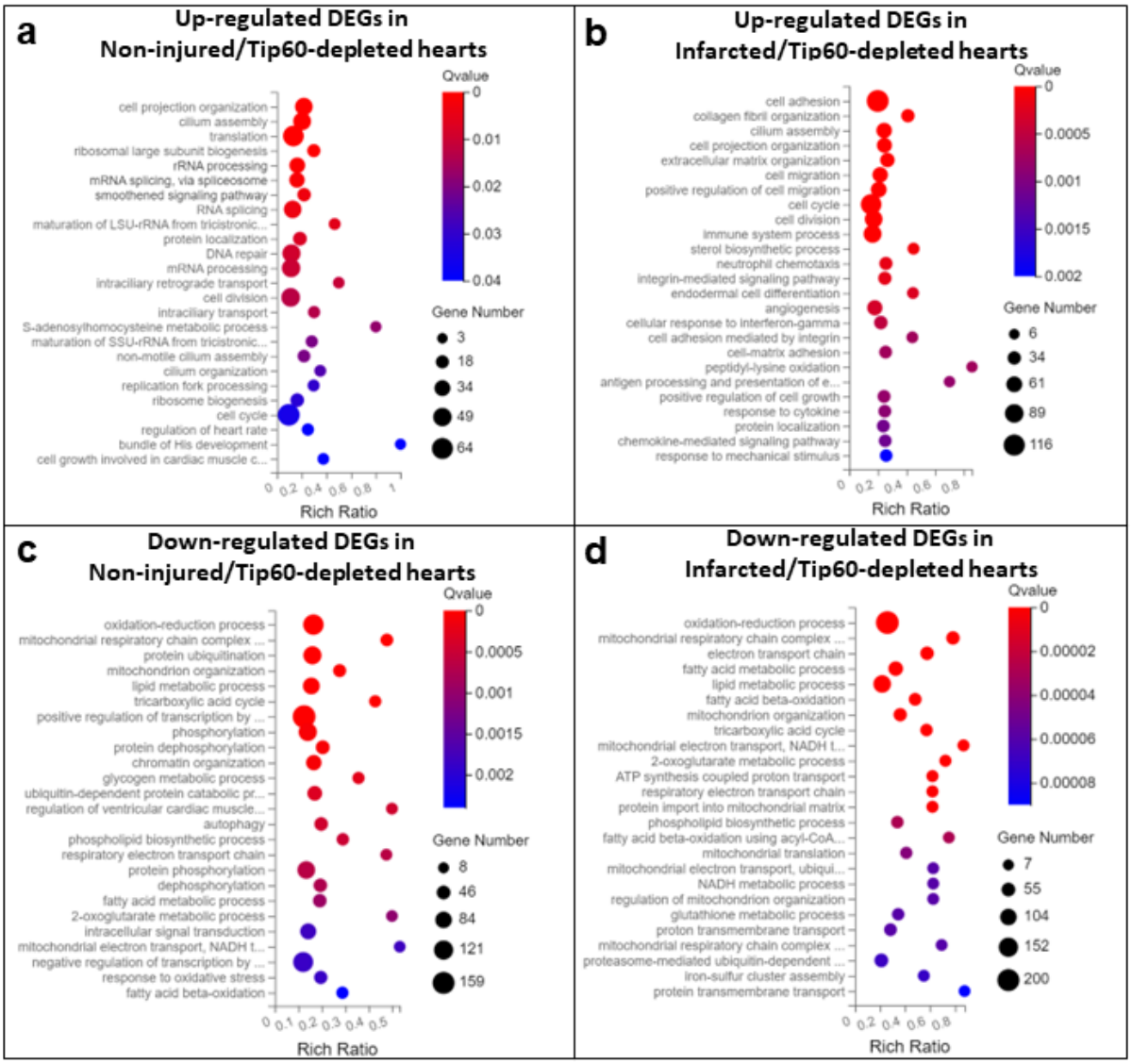

Figure 8. GO enrichment analysis of differentially expressed genes (DEGs) in non-injured versus infarcted hearts that were Tip60-depleted. Panels a-d: The top 25 GO terms that are significantly enriched in up- and down-regulated DEGs in naïve (respectively panels a and c), and infarcted (respectively panels b and d) Tip60-depleted hearts (*Kat5*$^{\Delta/\Delta}$) compared to controls (*Kat5*$^{f/f}$). Rich Ratio = the number of DEGs/total number of genes annotated to each GO term. The size of each bubble represents the number of DEGs annotated to a GO Term; colors represent the significance of enrichment.

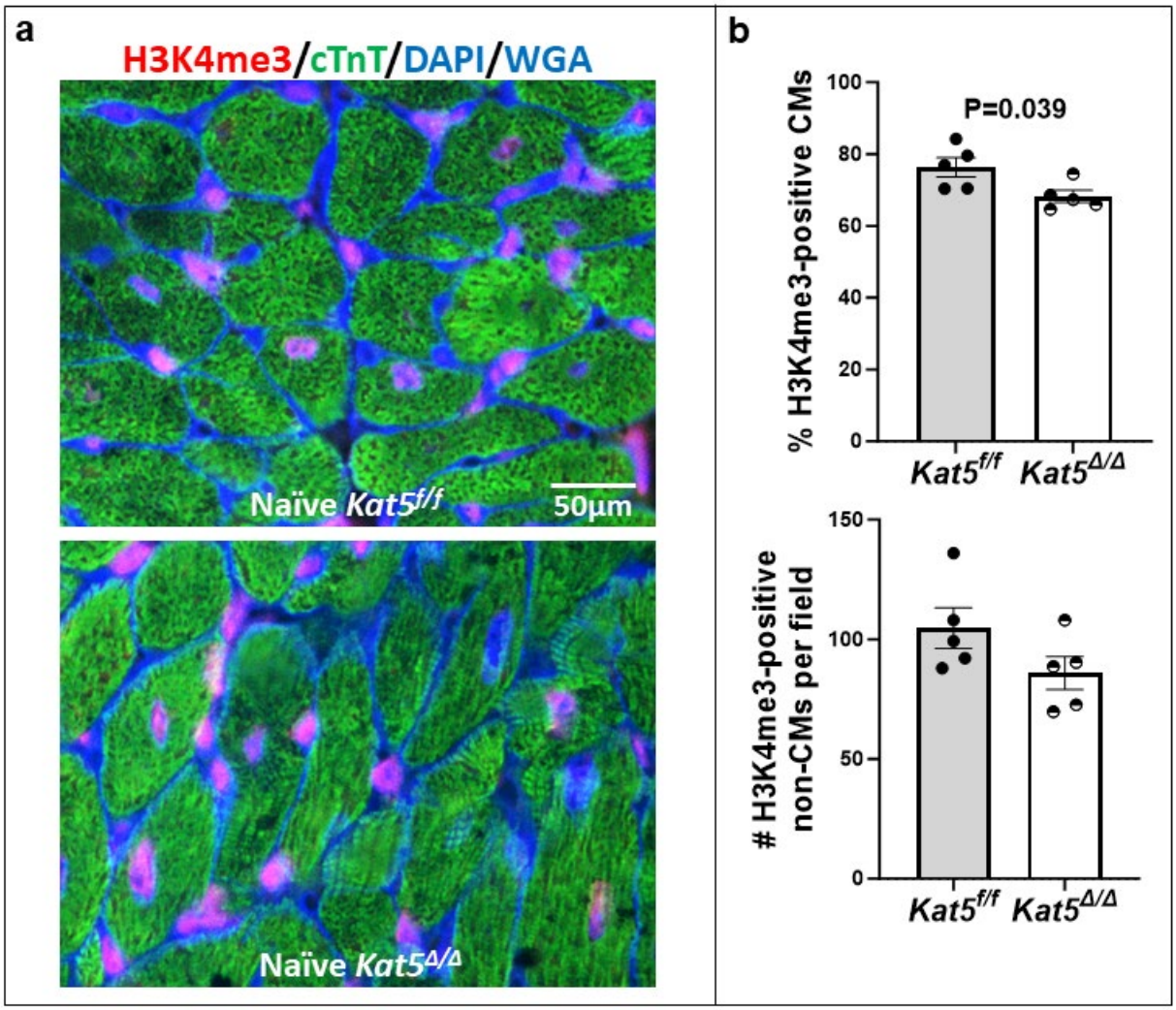

Figure 9. Reduced levels of trimethylated histone H3 (H3K4^{me3}) in Tip60-depleted Hearts. Panel a, representative immunostaining images of 13-week-old adult hearts in which Tip60 was depleted by treatment with tamoxifen for three consecutive days. Hearts were processed for immunostaining eleven days after the first injection. **Panel b**: Upper: Percentages of H3K4^{me3}-positive CMs enumerated in six randomly selected 400x cross-sectional fields. A minimum of 300 CMs were assessed in each heart. Lower: Numbers of H3K4^{me3}-positive non-CMs per 400x field. Bars denote means ±SEM. *P<0.05 vs. *Kat5$^{f/f}$* per unpaired Student's t-test. Each point represents a biological replicate (i.e., individual mouse heart).

SUPPLEMENTAL FIGURES & LEGENDS

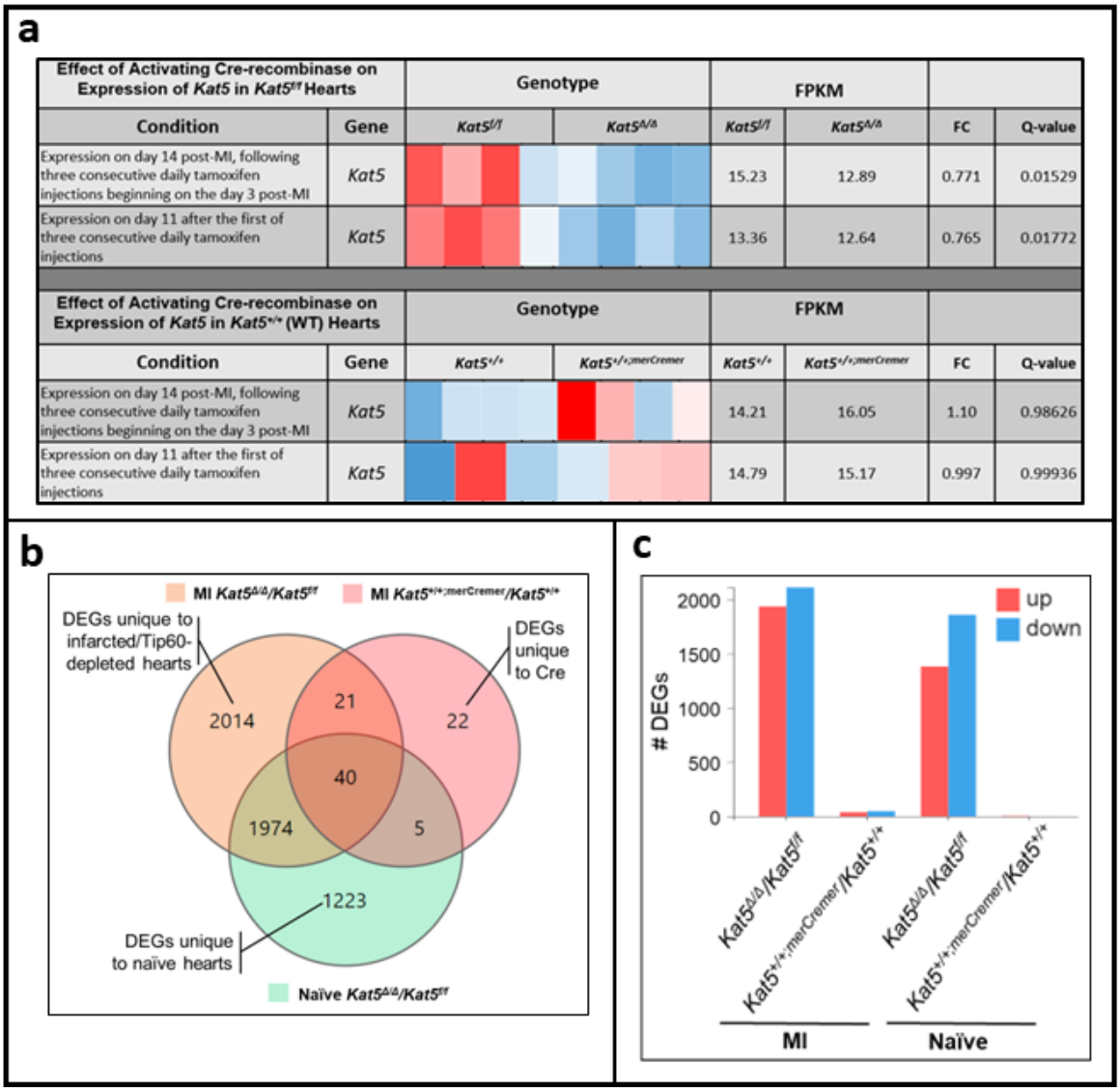

Supplemental Figure 1. Effects of Tip60 depletion on gene expression in infarcted and naïve hearts. Panel a: RNAseq results showing the extent of Tip60 depletion. Twelve-week-old *Kat5*$^{f/f}$, *Kat5*$^{\Delta/\Delta}$, *Kat5*$^{+/+}$, and *Kat5*$^{+/+;merCremer}$ mice were infarcted (see Methods). Beginning on the third day post-infarction, mice were intraperitoneally injected with 40 mg/kg tamoxifen for three consecutive days. On the 14th day post-infarction, hearts were collected and processed for total RNA. Naïve mice of similar age were intraperitoneally injected with 40 mg/kg tamoxifen for three consecutive days and hearts were collected and processed for RNA on the 11 day after the first injection. Each colored column represents a biological replicate. **Panel b:** Venn diagram depicting overlap of differentially expressed genes (DEGs) between different comparison groups. **Panel c:** Total number of up/down-regulated DEGs in naïve and infarcted hearts. Minimal off-target effects of Cre-recombinase were observed comparing *Kat5*$^{+/+}$ vs. *Kat5*$^{+/+;merCremer}$.

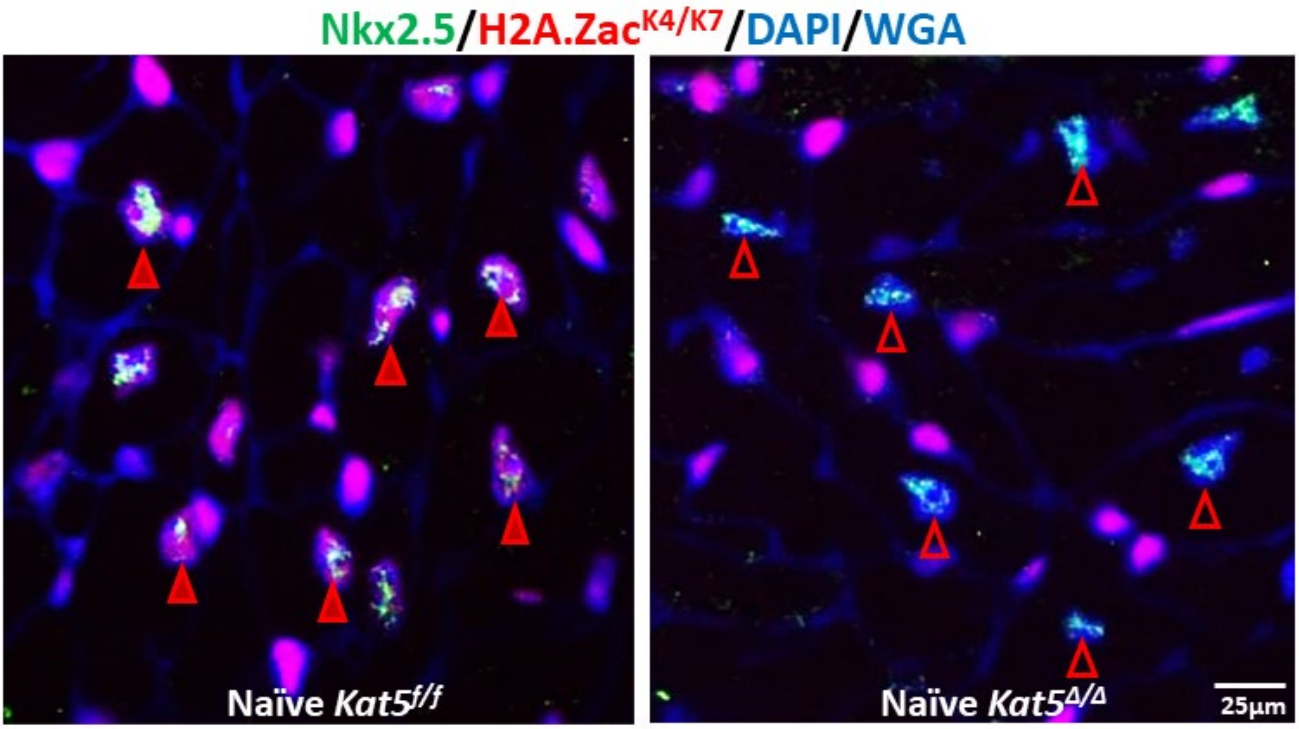

Supplemental Figure 2. Verification of cardiomyocyte identity by immunostaining Nkx2-5. Closed red arrowheads in naïve control (*Kat5*$^{f/f}$) myocardium denote CM nuclei containing acetylated H2A.Z (H2A.Zac$^{K4/K7}$). Open red arrowheads in naïve myocardium after Tip60 depletion (*Kat5*$^{Δ/Δ}$) denote CM nuclei devoid of acetylated H2A.Z. Punctate green fluorescent staining denotes Nkx2-5.

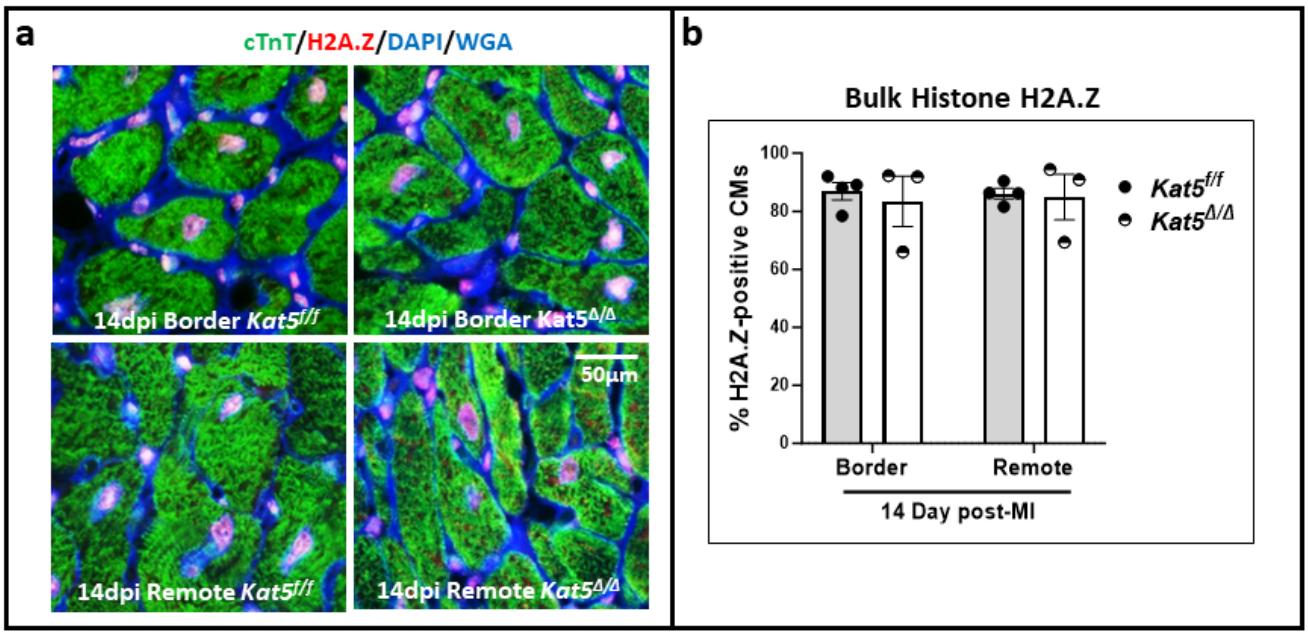

Supplemental Figure 3. Numbers of CMs containing bulk histone H2A.Z in infarcted hearts are unaffected by Tip60 depletion. Panel a, immunostaining bulk histone H2A.Z in CMs using anti-H2A.Z); CMs were identified using anti-cardiac troponin-T antibody. **Panel b**, percentages of CMs containing bulk H2A.Z were enumerated in six randomly selected 400x cross-sectional fields in the border zone and remote zone of each heart. For counting, total numbers of CMs and total numbers of H2A.Z-positive CMs were separately assessed at 400x magnification in six fields each within the border and remote zones; percentages of H2A.Z-positive CMs in each field were then averaged to obtain the percentages shown in panel b. *P<0.05 vs. *Kat5*$^{f/f}$ per unpaired Student's t-test; means ±SEM.

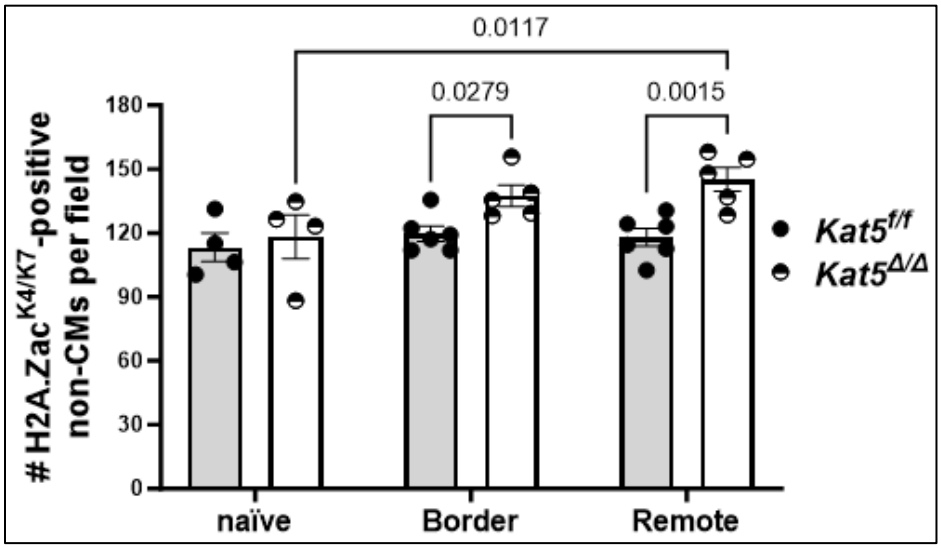

Supplemental Figure 4. Increased H2A.Zac$^{K4/K7}$-positive interstitial cells (i.e., non-CMs) in naïve and infarcted Tip60-depleted hearts. P values calculated by two-way ANOVA with Bonferroni's multiple comparisons; means ±SEM.

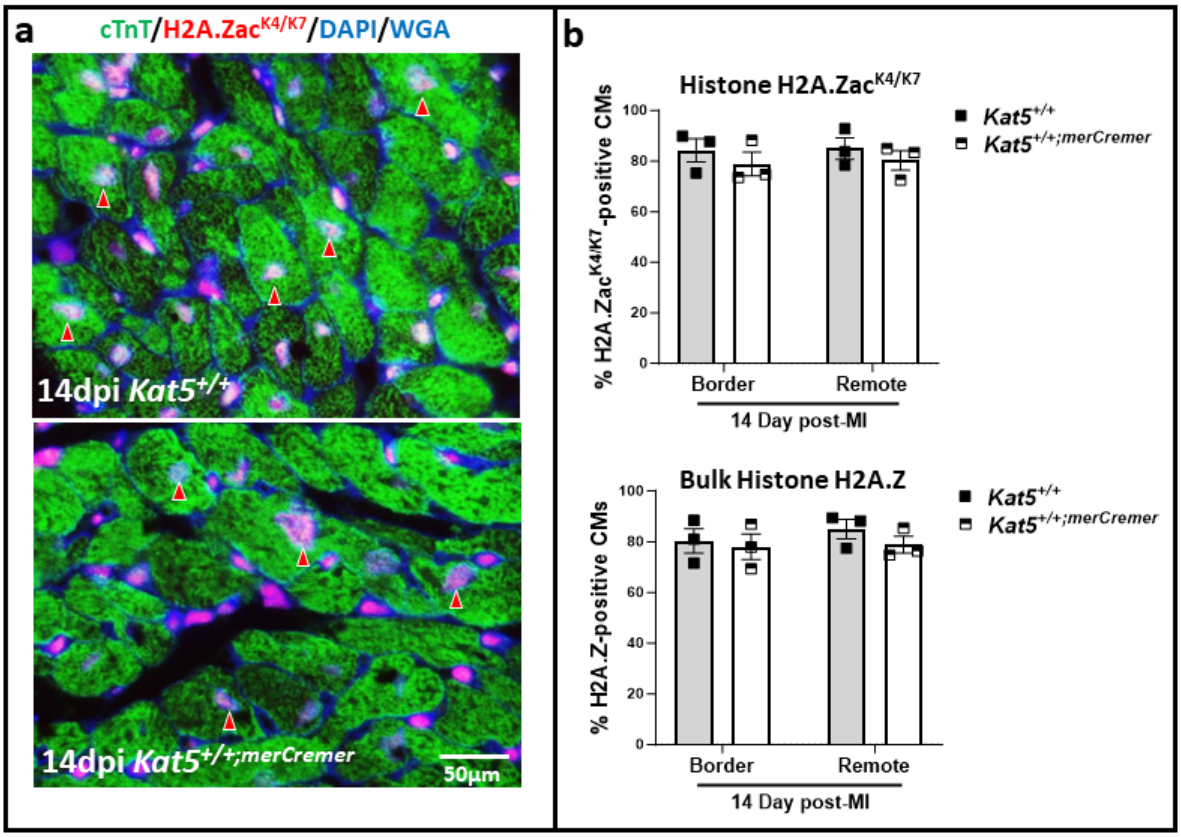

Supplemental Figure 5. Cre recombinase, alone, does not affect numbers of CMs containing H2A.Zac$^{K4/K7}$ or bulk histone H2A.Z in infarcted hearts. Panel a, typical immunostains showing H2A.Zac$^{K4/K7}$-positive (red fluorescence) nuclei in wild-type CMs (*Kat5*$^{+/+}$, above) and in CMs expressing tamoxifen-activated Cre-recombinase (*Kat5*$^{+/+;merCremer}$, below). Red arrowheads denote H2A.Zac$^{K4/K7}$-positive CMs. **Panel b** shows enumeration of H2A.Zac$^{K4/K7}$-positive CMs (above), as well as CMs enumerated for content of bulk histone H2A.Z (below). In both instances CMs were identified by immunostaining with anti-cardiac troponin-T (green fluorescence) combined with WGA. *P<0.05 vs. *Kat5*$^{+/+}$ per unpaired Student's t-test; means ±SEM.

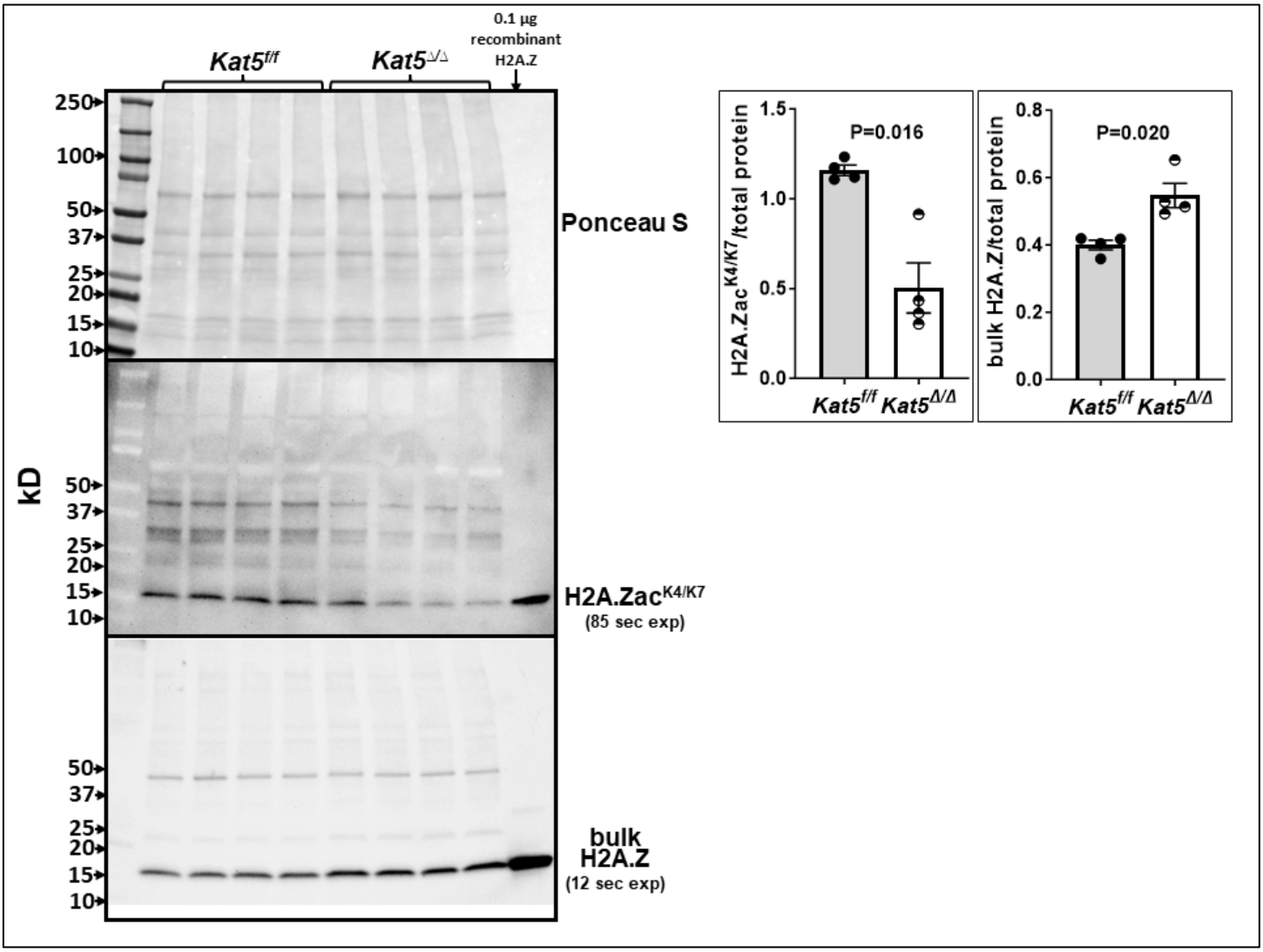

Supplemental Figure 6. Non-cropped western blots showing reduced levels of acetylated H2A.Z$^{K4/K7}$ in Tip60-depleted (*Kat5*$^{\Delta/\Delta}$) hearts. Each point represents a biological replicate (i.e., an individual mouse heart). According to the manufacturer (Cell Signaling Technology) of the anti-H2A.Zac$^{K4/K7}$ antibody, the ~22 kDa band represents mono-ubiquitinated H2A.Z.

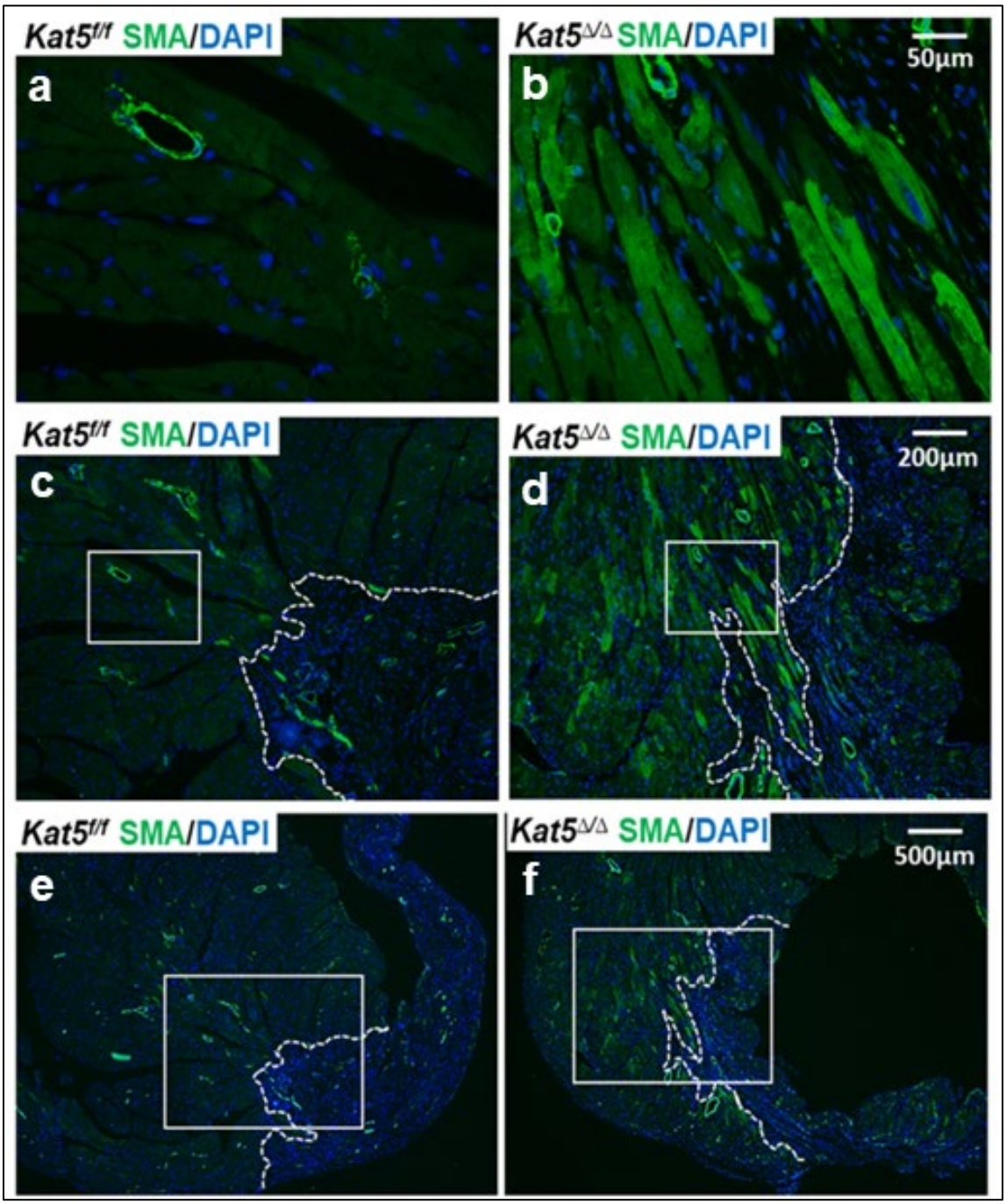

Supplemental Figure 7. Immunostains showing up-regulation of α-smooth muscle actin (α-sma) in CMs within the border zone of infarcted/Tip60-depleted hearts. Panels a-f are representative images of control ($Kat5^{f/f}$) and Tip60-depleted ($Kat5^{\Delta/\Delta}$) hearts at 28 days post-MI. Striated, α-sma-positive CMs are aligned along the border zone of Tip60-depleted hearts. **Panels a-b** are shown at reduced magnifications in the white rectangles in panels c-f. The broken white line in panels c-f demarcates the border and infarct zones.

REFERENCES

1. Tsao CW, Aday AW, Almarzooq ZI, Alonso A, Beaton AZ, Bittencourt MS, Boehme AK, Buxton AE, Carson AP, Commodore-Mensah Y, Elkind MSV, Evenson KR, Eze-Nliam C, Ferguson JF, Generoso G, Ho JE, Kalani R, Khan SS, Kissela BM, Knutson KL, Levine DA, Lewis TT, Liu J, Loop MS, Ma J, Mussolino ME, Navaneethan SD, Perak AM, Poudel R, Rezk-Hanna M, Roth GA, Schroeder EB, Shah SH, Thacker EL, VanWagner LB, Virani SS, Voecks JH, Wang NY, Yaffe K and Martin SS. Heart Disease and Stroke Statistics-2022 Update: A Report From the American Heart Association. *Circulation*. 2022;145:e153-e639.
2. Sadek H and Olson EN. Toward the Goal of Human Heart Regeneration. *Cell Stem Cell*. 2020;26:7-16.
3. Lee MS, Seo J, Choi DY, Lee EW, Ko A, Ha NC, Yoon JB, Lee HW, Kim KP and Song J. Stabilization of p21 (Cip1/WAF1) following Tip60-dependent acetylation is required for p21-mediated DNA damage response. *Cell death and differentiation*. 2013;20:620-9.
4. Li B, Hu Y, Li X, Jin G, Chen X, Chen G, Chen Y, Huang S, Liao W, Liao Y, Teng Z and Bin J. Sirt1 Antisense Long Noncoding RNA Promotes Cardiomyocyte Proliferation by Enhancing the Stability of Sirt1. *J Am Heart Assoc*. 2018;7:e009700.
5. Sun Y, Jiang X, Chen S, Fernandes N and Price BD. A role for the Tip60 histone acetyltransferase in the acetylation and activation of ATM. *Proc Natl Acad Sci U S A*. 2005;102:13182-7.
6. Bose A, Sudevan S, Rao VJ, Shima H, Trivedi AK, Igarashi K and Kundu TK. Haploinsufficient tumor suppressor Tip60 negatively regulates oncogenic Aurora B kinase. *J Biosci*. 2019;44.
7. Sykes SM, Mellert HS, Holbert MA, Li K, Marmorstein R, Lane WS and McMahon SB. Acetylation of the p53 DNA-binding domain regulates apoptosis induction. *Mol Cell*. 2006;24:841-51.
8. Tang Y, Luo J, Zhang W and Gu W. Tip60-dependent acetylation of p53 modulates the decision between cell-cycle arrest and apoptosis. *Mol Cell*. 2006;24:827-39.
9. Tang Y, Zhao W, Chen Y, Zhao Y and Gu W. Acetylation is indispensable for p53 activation. *Cell*. 2008;133:612-26.
10. Wang X, Lupton C, Lauth A, Wan TC, Foster P, Patterson M, Auchampach JA and Lough JW. Evidence that the acetyltransferase Tip60 induces the DNA damage response and cell-cycle arrest in neonatal cardiomyocytes. *J Mol Cell Cardiol*. 2021.
11. Wang X, Wan TC, Lauth A, Purdy AL, Kulik KR, Patterson M, Lough JW and Auchampach JA. Conditional depletion of the acetyltransferase Tip60 protects against the damaging effects of myocardial infarction. *J Mol Cell Cardiol*. 2022;163:9-19.
12. Wang X, Wan TC, Kulik KR, Lauth A, Smith BC, Lough JW and Auchampach JA. Pharmacological inhibition of the acetyltransferase Tip60 mitigates myocardial infarction injury. *Dis Model Mech*. 2023;16.
13. Kubin T, Poling J, Kostin S, Gajawada P, Hein S, Rees W, Wietelmann A, Tanaka M, Lorchner H, Schimanski S, Szibor M, Warnecke H and Braun T. Oncostatin M is a major mediator of cardiomyocyte dedifferentiation and remodeling. *Cell Stem Cell*. 2011;9:420-32.
14. D'Uva G, Aharonov A, Lauriola M, Kain D, Yahalom-Ronen Y, Carvalho S, Weisinger K, Bassat E, Rajchman D, Yifa O, Lysenko M, Konfino T, Hegesh J, Brenner O, Neeman M, Yarden Y, Leor J, Sarig R, Harvey RP and Tzahor E. ERBB2 triggers mammalian heart regeneration by promoting cardiomyocyte dedifferentiation and proliferation. *Nat Cell Biol*. 2015;17:627-38.
15. Valussi M, Besser J, Wystub-Lis K, Zukunft S, Richter M, Kubin T, Boettger T and Braun T. Repression of Osmr and Fgfr1 by miR-1/133a prevents cardiomyocyte dedifferentiation and cell cycle entry in the adult heart. *Sci Adv*. 2021;7:eabi6648.
16. Avraham Shakked ZP, Alla Aharonov, Matteo Ghiringhelli, Kfir-Baruch Umansky, David Kain, Jacob Elkahal, Yalin Divinsky, Phong Dang Nguyen, Shoval Miyara, Gilgi Friedlander, Alon Savidor, Lingling Zhang, Dahlia E. Perez, Rachel Sarig, Daria Lendengolts, Hanna Bueno-Levy, Nathaniel Kastan, Yishai Levin, Jeroen Bakkers, Lior Gepstein & Eldad Tzahor. Redifferentiated cardiomyocytes retain residual dedifferentiation signatures are are protected from ischemic injury. *Nature Cardiovascular Research*. 2023;2:383-398.
17. Yahalom-Ronen Y, Rajchman D, Sarig R, Geiger B and Tzahor E. Reduced matrix rigidity promotes neonatal cardiomyocyte dedifferentiation, proliferation and clonal expansion. *eLife*. 2015;4.
18. Bassat E, Mutlak YE, Genzelinakh A, Shadrin IY, Baruch Umansky K, Yifa O, Kain D, Rajchman D, Leach J, Riabov Bassat D, Udi Y, Sarig R, Sagi I, Martin JF, Bursac N, Cohen S and Tzahor E. The extracellular matrix protein agrin promotes heart regeneration in mice. *Nature*. 2017;547:179-184.

19. Williams C, Quinn KP, Georgakoudi I and Black LD, 3rd. Young developmental age cardiac extracellular matrix promotes the expansion of neonatal cardiomyocytes in vitro. *Acta biomaterialia*. 2014;10:194-204.
20. Notari M, Ventura-Rubio A, Bedford-Guaus SJ, Jorba I, Mulero L, Navajas D, Marti M and Raya A. The local microenvironment limits the regenerative potential of the mouse neonatal heart. *Sci Adv*. 2018;4:eaao5553.
21. Li X, Wu F, Gunther S, Looso M, Kuenne C, Zhang T, Wiesnet M, Klatt S, Zukunft S, Fleming I, Poschet G, Wietelmann A, Atzberger A, Potente M, Yuan X and Braun T. Inhibition of fatty acid oxidation enables heart regeneration in adult mice. *Nature*. 2023.
22. Beisaw A and Wu CC. Cardiomyocyte maturation and its reversal during cardiac regeneration. *Dev Dyn*. 2022.
23. Numata A, Kwok HS, Zhou QL, Li J, Tirado-Magallanes R, Angarica VE, Hannah R, Park J, Wang CQ, Krishnan V, Rajagopalan D, Zhang Y, Zhou S, Welner RS, Osato M, Jha S, Bohlander SK, Gottgens B, Yang H, Benoukraf T, Lough JW, Bararia D and Tenen DG. Lysine acetyltransferase Tip60 is required for hematopoietic stem cell maintenance. *Blood*. 2020;136:1735-1747.
24. Janas JA, Zhang L, Luu JH, Demeter J, Meng L, Marro SG, Mall M, Mooney NA, Schaukowitch K, Ng YH, Yang N, Huang Y, Neumayer G, Gozani O, Elias JE, Jackson PK and Wernig M. Tip60-mediated H2A.Z acetylation promotes neuronal fate specification and bivalent gene activation. *Mol Cell*. 2022.
25. Fisher JB, Horst A, Wan T, Kim MS, Auchampach J and Lough J. Depletion of Tip60 from In Vivo Cardiomyocytes Increases Myocyte Density, Followed by Cardiac Dysfunction, Myocyte Fallout and Lethality. *PLoS One*. 2016;11:e0164855.
26. Sohal DS, Nghiem M, Crackower MA, Witt SA, Kimball TR, Tymitz KM, Penninger JM and Molkentin JD. Temporally regulated and tissue-specific gene manipulations in the adult and embryonic heart using a tamoxifen-inducible Cre protein. *Circ Res*. 2001;89:20-5.
27. Wang X, Wan TC, Lauth A, Purdy AL, Kulik KR, Patterson M, Lough JW and Auchampach JA. Conditional depletion of the acetyltransferase Tip60 protects against the damaging effects of myocardial infarction. *J Mol Cell Cardiol*. 2021;163:9-19.
28. Tzahor E and Dimmeler S. A coalition to heal-the impact of the cardiac microenvironment. *Science*. 2022;377:eabm4443.
29. Chen Y, Luttmann FF, Schoger E, Scholer HR, Zelarayan LC, Kim KP, Haigh JJ, Kim J and Braun T. Reversible reprogramming of cardiomyocytes to a fetal state drives heart regeneration in mice. *Science*. 2021;373:1537-1540.
30. Tabula Muris C, Overall c, Logistical c, Organ c, processing, Library p, sequencing, Computational data a, Cell type a, Writing g, Supplemental text writing g and Principal i. Single-cell transcriptomics of 20 mouse organs creates a Tabula Muris. *Nature*. 2018;562:367-372.
31. Aharonov A, Shakked A, Umansky KB, Savidor A, Genzelinakh A, Kain D, Lendengolts D, Revach OY, Morikawa Y, Dong J, Levin Y, Geiger B, Martin JF and Tzahor E. ERBB2 drives YAP activation and EMT-like processes during cardiac regeneration. *Nat Cell Biol*. 2020;22:1346-1356.
32. Fan X, Hughes BG, Ali MA, Cho WJ, Lopez W and Schulz R. Dynamic Alterations to alpha-Actinin Accompanying Sarcomere Disassembly and Reassembly during Cardiomyocyte Mitosis. *PLoS One*. 2015;10:e0129176.
33. Sun Y, Sun J, Lungchukiet P, Quarni W, Yang S, Zhang X and Bai W. Fe65 Suppresses Breast Cancer Cell Migration and Invasion through Tip60 Mediated Cortactin Acetylation. *Sci Rep*. 2015;5:11529.
34. Ammer AG and Weed SA. Cortactin branches out: roles in regulating protrusive actin dynamics. *Cell Motil Cytoskeleton*. 2008;65:687-707.
35. Ren G, Crampton MS and Yap AS. Cortactin: Coordinating adhesion and the actin cytoskeleton at cellular protrusions. *Cell Motil Cytoskeleton*. 2009;66:865-73.
36. Hertig V, Matos-Nieves A, Garg V, Villeneuve L, Mamarbachi M, Caland L and Calderone A. Nestin expression is dynamically regulated in cardiomyocytes during embryogenesis. *J Cell Physiol*. 2018;233:3218-3229.
37. Herrer I, Rosello-Lleti E, Rivera M, Molina-Navarro MM, Tarazon E, Ortega A, Martinez-Dolz L, Trivino JC, Lago F, Gonzalez-Juanatey JR, Bertomeu V, Montero JA and Portoles M. RNA-sequencing analysis reveals new alterations in cardiomyocyte cytoskeletal genes in patients with heart failure. *Lab Invest*. 2014;94:645-53.
38. Chang AN, Mahajan P, Knapp S, Barton H, Sweeney HL, Kamm KE and Stull JT. Cardiac myosin light chain is phosphorylated by Ca2+/calmodulin-dependent and -independent kinase activities. *Proc Natl Acad Sci U S A*. 2016;113:E3824-33.

39. Kubin T, Gajawada P, Bramlage P, Hein S, Berge B, Cetinkaya A, Burger H, Schonburg M, Schaper W, Choi YH and Richter M. The Role of Oncostatin M and Its Receptor Complexes in Cardiomyocyte Protection, Regeneration, and Failure. *International journal of molecular sciences*. 2022;23.
40. Durbin MD, O'Kane J, Lorentz S, Firulli AB and Ware SM. SHROOM3 is downstream of the planar cell polarity pathway and loss-of-function results in congenital heart defects. *Dev Biol*. 2020;464:124-136.
41. Bedada FB, Chan SS, Metzger SK, Zhang L, Zhang J, Garry DJ, Kamp TJ, Kyba M and Metzger JM. Acquisition of a quantitative, stoichiometrically conserved ratiometric marker of maturation status in stem cell-derived cardiac myocytes. *Stem Cell Reports*. 2014;3:594-605.
42. VanDusen NJ, Lee JY, Gu W, Butler CE, Sethi I, Zheng Y, King JS, Zhou P, Suo S, Guo Y, Ma Q, Yuan GC and Pu WT. Massively parallel in vivo CRISPR screening identifies RNF20/40 as epigenetic regulators of cardiomyocyte maturation. *Nature communications*. 2021;12:4442.
43. Itou J, Oishi I, Kawakami H, Glass TJ, Richter J, Johnson A, Lund TC and Kawakami Y. Migration of cardiomyocytes is essential for heart regeneration in zebrafish. *Development*. 2012;139:4133-42.
44. Zhang R, Han P, Yang H, Ouyang K, Lee D, Lin YF, Ocorr K, Kang G, Chen J, Stainier DY, Yelon D and Chi NC. In vivo cardiac reprogramming contributes to zebrafish heart regeneration. *Nature*. 2013;498:497-501.
45. Morikawa Y, Zhang M, Heallen T, Leach J, Tao G, Xiao Y, Bai Y, Li W, Willerson JT and Martin JF. Actin cytoskeletal remodeling with protrusion formation is essential for heart regeneration in Hippo-deficient mice. *Science signaling*. 2015;8:ra41.
46. Kuhn B, del Monte F, Hajjar RJ, Chang YS, Lebeche D, Arab S and Keating MT. Periostin induces proliferation of differentiated cardiomyocytes and promotes cardiac repair. *Nat Med*. 2007;13:962-9.
47. Luxan G and Dimmeler S. The vasculature: a therapeutic target in heart failure? *Cardiovasc Res*. 2022;118:53-64.
48. Rasi K, Piuhola J, Czabanka M, Sormunen R, Ilves M, Leskinen H, Rysa J, Kerkela R, Janmey P, Heljasvaara R, Peuhkurinen K, Vuolteenaho O, Ruskoaho H, Vajkoczy P, Pihlajaniemi T and Eklund L. Collagen XV is necessary for modeling of the extracellular matrix and its deficiency predisposes to cardiomyopathy. *Circ Res*. 2010;107:1241-52.
49. Rhee S, Paik DT, Yang JY, Nagelberg D, Williams I, Tian L, Roth R, Chandy M, Ban J, Belbachir N, Kim S, Zhang H, Phansalkar R, Wong KM, King DA, Valdez C, Winn VD, Morrison AJ, Wu JC and Red-Horse K. Endocardial/endothelial angiocrines regulate cardiomyocyte development and maturation and induce features of ventricular non-compaction. *Eur Heart J*. 2021;42:4264-4276.
50. Baehr A, Umansky KB, Bassat E, Jurisch V, Klett K, Bozoglu T, Hornaschewitz N, Solyanik O, Kain D, Ferraro B, Cohen-Rabi R, Krane M, Cyran C, Soehnlein O, Laugwitz KL, Hinkel R, Kupatt C and Tzahor E. Agrin Promotes Coordinated Therapeutic Processes Leading to Improved Cardiac Repair in Pigs. *Circulation*. 2020;142:868-881.
51. Inai K. Atrioventricular Valve Abnormalities: From Molecular Mechanisms Underlying Morphogenesis to Clinical Perspective. In: T. Nakanishi, R. R. Markwald, H. S. Baldwin, B. B. Keller, D. Srivastava and H. Yamagishi, eds. *Etiology and Morphogenesis of Congenital Heart Disease: From Gene Function and Cellular Interaction to Morphology* Tokyo; 2016: 135-43.
52. Stohn JP, Perreault NG, Wang Q, Liaw L and Lindner V. Cthrc1, a novel circulating hormone regulating metabolism. *PLoS One*. 2012;7:e47142.
53. Nordquist EM, Dutta P, Kodigepalli KM, Mattern C, McDermott MR, Trask AJ, LaHaye S, Lindner V and Lincoln J. Tgfbeta1-Cthrc1 Signaling Plays an Important Role in the Short-Term Reparative Response to Heart Valve Endothelial Injury. *Arteriosclerosis, thrombosis, and vascular biology*. 2021;41:2923-2942.
54. Ruiz-Villalba A, Romero JP, Hernandez SC, Vilas-Zornoza A, Fortelny N, Castro-Labrador L, San Martin-Uriz P, Lorenzo-Vivas E, Garcia-Olloqui P, Palacio M, Gavira JJ, Bastarrika G, Janssens S, Wu M, Iglesias E, Abizanda G, de Morentin XM, Lasaga M, Planell N, Bock C, Alignani D, Medal G, Prudovsky I, Jin YR, Ryzhov S, Yin H, Pelacho B, Gomez-Cabrero D, Lindner V, Lara-Astiaso D and Prosper F. Single-Cell RNA Sequencing Analysis Reveals a Crucial Role for CTHRC1 (Collagen Triple Helix Repeat Containing 1) Cardiac Fibroblasts After Myocardial Infarction. *Circulation*. 2020;142:1831-1847.
55. Maroli G and Braun T. The long and winding road of cardiomyocyte maturation. *Cardiovasc Res*. 2021;117:712-726.
56. Honkoop H, de Bakker DE, Aharonov A, Kruse F, Shakked A, Nguyen PD, de Heus C, Garric L, Muraro MJ, Shoffner A, Tessadori F, Peterson JC, Noort W, Bertozzi A, Weidinger G, Posthuma G, Grun D, van der Laarse WJ, Klumperman J, Jaspers RT, Poss KD, van Oudenaarden A, Tzahor E and Bakkers J. Single-cell analysis

uncovers that metabolic reprogramming by ErbB2 signaling is essential for cardiomyocyte proliferation in the regenerating heart. *eLife*. 2019;8.
57. Li X, Wu F, Gunther S, Looso M, Kuenne C, Zhang T, Wiesnet M, Klatt S, Zukunft S, Fleming I, Poschet G, Wietelmann A, Atzberger A, Potente M, Yuan X and Braun T. Inhibition of fatty acid oxidation enables heart regeneration in adult mice. *Nature*. 2023;622:619-626.
58. Janas JA, Zhang L, Luu JH, Demeter J, Meng L, Marro SG, Mall M, Mooney NA, Schaukowitch K, Ng YH, Yang N, Huang Y, Neumayer G, Gozani O, Elias JE, Jackson PK and Wernig M. Tip60-mediated H2A.Z acetylation promotes neuronal fate specification and bivalent gene activation. *Mol Cell*. 2022;82:4627-4646 e14.
59. Ikeda S, Mizushima W, Sciarretta S, Abdellatif M, Zhai P, Mukai R, Fefelova N, Oka SI, Nakamura M, Del Re DP, Farrance I, Park JY, Tian B, Xie LH, Kumar M, Hsu CP, Sadayappan S, Shimokawa H, Lim DS and Sadoshima J. Hippo Deficiency Leads to Cardiac Dysfunction Accompanied by Cardiomyocyte Dedifferentiation During Pressure Overload. *Circ Res*. 2019;124:292-305.
60. Zhu Y, Do VD, Richards AM and Foo R. What we know about cardiomyocyte dedifferentiation. *J Mol Cell Cardiol*. 2021;152:80-91.
61. Bongiovanni C, Sacchi F, Da Pra S, Pantano E, Miano C, Morelli MB and D'Uva G. Reawakening the Intrinsic Cardiac Regenerative Potential: Molecular Strategies to Boost Dedifferentiation and Proliferation of Endogenous Cardiomyocytes. *Front Cardiovasc Med*. 2021;8:750604.
62. Law C and Cheung P. Expression of Non-acetylatable H2A.Z in Myoblast Cells Blocks Myoblast Differentiation through Disruption of MyoD Expression. *J Biol Chem*. 2015;290:13234-49.
63. Yao F, Yu P, Li Y, Yuan X, Li Z, Zhang T, Liu F, Wang Y, Wang Y, Li D, Ma B, Shu C, Kong W, Zhou B and Wang L. Histone Variant H2A.Z Is Required for the Maintenance of Smooth Muscle Cell Identity as Revealed by Single-Cell Transcriptomics. *Circulation*. 2018;138:2274-2288.
64. Uscategui Calderon M, Gonzalez BA and Yutzey KE. Cardiomyocyte-fibroblast crosstalk in the postnatal heart. *Front Cell Dev Biol*. 2023;11:1163331.
65. Durmus T, LeClair RJ, Park KS, Terzic A, Yoon JK and Lindner V. Expression analysis of the novel gene collagen triple helix repeat containing-1 (Cthrc1). *Gene Expr Patterns*. 2006;6:935-40.
66. Liu YJ, Du J, Li J, Tan XP and Zhang Q. CTHRC1, a novel gene with multiple functions in physiology, disease and solid tumors (Review). *Oncol Lett*. 2023;25:266.
67. Pyagay P, Heroult M, Wang Q, Lehnert W, Belden J, Liaw L, Friesel RE and Lindner V. Collagen triple helix repeat containing 1, a novel secreted protein in injured and diseased arteries, inhibits collagen expression and promotes cell migration. *Circ Res*. 2005;96:261-8.
68. Elia A, Mohsin S and Khan M. Cardiomyocyte Ploidy, Metabolic Reprogramming and Heart Repair. *Cells*. 2023;12.
69. Liao R, Jain M, Cui L, D'Agostino J, Aiello F, Luptak I, Ngoy S, Mortensen RM and Tian R. Cardiac-specific overexpression of GLUT1 prevents the development of heart failure attributable to pressure overload in mice. *Circulation*. 2002;106:2125-31.
70. Tang Z, Wang K, Lo L and Chen J. Tg(Delta113p53:cmyc) Transgene Upregulates glut1 Expression to Promote Zebrafish Heart Regeneration. *J Cardiovasc Dev Dis*. 2023;10.
71. Fajardo VM, Feng I, Chen BY, Perez-Ramirez CA, Shi B, Clark P, Tian R, Lien CL, Pellegrini M, Christofk H, Nakano H and Nakano A. GLUT1 overexpression enhances glucose metabolism and promotes neonatal heart regeneration. *Sci Rep*. 2021;11:8669.
72. Auchampach J, Han L, Huang GN, Kuhn B, Lough JW, O'Meara CC, Payumo AY, Rosenthal NA, Sucov HM, Yutzey KE and Patterson M. Measuring cardiomyocyte cell-cycle activity and proliferation in the age of heart regeneration. *Am J Physiol Heart Circ Physiol*. 2022;322:H579-H596.
73. Purdy AL, Swift SK, Sucov HM and Patterson M. Tnni3k influences cardiomyocyte S-phase activity and proliferation. *J Mol Cell Cardiol*. 2023;183:22-26.
74. Liu L, Li RG and Martin JF. An improved method reveals the dual role of Tnni3k in promoting S-phase entry while suppressing cell division in cardiomyocytes. *J Mol Cell Cardiol*. 2023;183:100-101.
75. Kim CH, Kim JW, Jang SM, An JH, Seo SB and Choi KH. The chromodomain-containing histone acetyltransferase TIP60 acts as a code reader, recognizing the epigenetic codes for initiating transcription. *Bioscience, biotechnology, and biochemistry*. 2015;79:532-8.
76. Jang SM, Kim JW, Kim CH, An JH, Johnson A, Song PI, Rhee S and Choi KH. KAT5-mediated SOX4 acetylation orchestrates chromatin remodeling during myoblast differentiation. *Cell death & disease*. 2015;6:e1857.

77. Sun Y, Jiang X, Xu Y, Ayrapetov MK, Moreau LA, Whetstine JR and Price BD. Histone H3 methylation links DNA damage detection to activation of the tumour suppressor Tip60. *Nat Cell Biol*. 2009;11:1376-82.
78. Wang X, Lauth A, Wan TC, Lough JW and Auchampach JA. Myh6-driven Cre-recombinase activates the DNA damage response and the cell-cycle in the myocardium in the absence of loxP sites. *Dis Model Mech*. 2020.